CHAPTER

4

MULTIDIMENSIONAL NMR SPECTROSCOPY

In the simplest pulsed NMR experiment, transverse magnetization excited by an rf pulse is sampled and stored at regular intervals during the *acquisition period* to generate a digital representation of the FID. Fourier transformation of the digitized signal yields the conventional one-dimensional spectrum (Chapter 3). In more complex one-dimensional NMR experiments, perturbations, which usually take the form of applied rf fields, are imposed on the spin system during the acquisition period or during a *preparation period* that precedes the acquisition period. Comparison of the spectra obtained in the presence and absence of the perturbations then yields information on the properties of the spin system affected. For example, weak irradiation of a particular spin during the acquisition period of a spin tickling experiment (*1, 2*) alters the natural multiplet patterns of spins that are scalar coupled to the irradiated spin. As another example, selective saturation of the resonance of a particular spin during the preparation period of a nuclear Overhauser effect NOE difference experiment (*3, 4*) alters the normal intensities of nearby, dipolar-coupled spins.

Unfortunately, one-dimensional NMR techniques, such as spin tickling, selective decoupling (*2, 5–7*), and NOE difference experiments, which yield extremely useful information in small molecules, are of limited applicability to the complex, highly overlapped spectra of

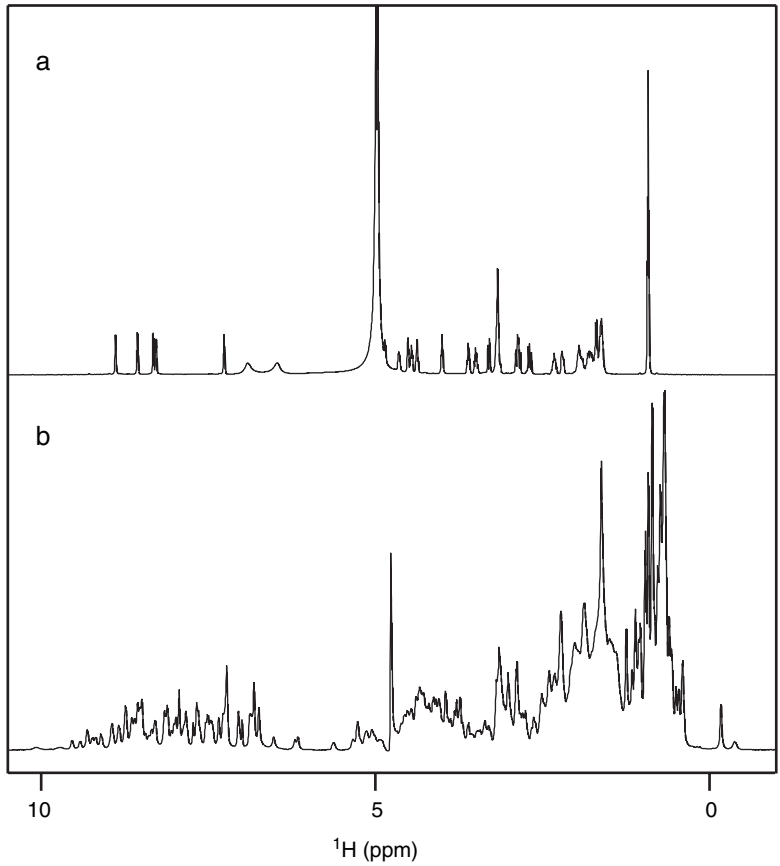

FIGURE 4.1 One-dimensional 500-MHz ^{1}H NMR spectra of (a) a hexapeptide at 280 K and (b) ubiquitin at 300 K. Samples were prepared in 90%/10% H_2O/D_2O. The two data sets were recorded at different temperatures; therefore, the water resonance signal appears at different chemical shifts in the two spectra.

biological macromolecules. By way of illustration, Fig. 4.1a shows the one-dimensional ^{1}H spectrum of a hexapeptide. Virtually all of the ^{1}H (multiplet) resonances are resolved; consequently, the assignment of each resonance to a particular ^{1}H spin in the molecule is straightforward and perturbations to the spectrum that result from selective irradiation of particular spins are easily detected. On the other hand, Fig. 4.1b shows a one-dimensional ^{1}H spectrum of the protein ubiquitin ($M_r = 8565$).

Several hundred ^1H resonances are crowded into approximately the same spectral region as the few peptide resonances. Because many resonances are degenerate, the signals are impossible to assign by using one-dimensional techniques, and selective perturbations to particular spins are difficult to achieve or detect experimentally. To effectively utilize the information available from NMR spectroscopy of biological macromolecules, a general method is required for improving resolution, facilitating resonance assignments, and detecting the effects of interactions between spins in complex NMR spectra. The explosive growth in the application of NMR spectroscopy to biological macromolecules in the past three decades attests to the success of multidimensional experiments in achieving these objectives.

4.1 Two-Dimensional NMR Spectroscopy

Initially, multidimensional NMR spectroscopy is introduced here by concentrating on two-dimensional spectroscopy. The overall structure of two-dimensional NMR experiments is presented, the separation of interactions into more than one frequency dimension is discussed, and techniques for selection of coherence transfer pathways are introduced. All of the methods and principles presented can be extended into higher dimensions in a straightforward manner. Specific multidimensional NMR experiments are discussed in Chapters 6–8.

In two-dimensional spectroscopy, two new elements, known as the *evolution* and *mixing periods*, are introduced into the NMR experiment between the preparation and acquisition periods. Thus, a general scheme for recording two-dimensional spectra is segmented into the four distinct parts illustrated in Fig. 4.2. The evolution period contains a variable time delay that is increased during the course of a two-dimensional NMR experiment from an initial value to a final value in m (usually equal) increments. For each of the m values of the incrementable delay, the same pulse sequence is executed twice (necessary for quadrature detection, as discussed in Section 4.3.4) and two FIDs, each consisting of n digitized complex data points, are

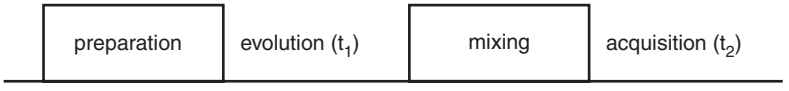

FIGURE 4.2 General scheme for two-dimensional NMR spectroscopy. The two-dimensional NMR experiment is divided into four defined components: preparation, evolution, mixing, and acquisition.

recorded. Each FID consists of p co-added transients for signal averaging or phase cycling. Thus, a total of $2 \times m \times p$ separate transients are recorded during the two-dimensional experiment, and a data array, which takes the form of either an m (complex) $\times$ n (complex) matrix or a $2m$ (real) $\times$ n (complex) matrix, is generated as a function of the two separate, independent time periods. Herein, the acquisition time (when the receiver is turned on and actually detects signal) is designated t_2, while the *indirect evolution* time is designated t_1. The rows of the data matrix represent data collected for a fixed t_1 value and different t_2 values, while the columns represent data collected for a fixed t_2 value and varying t_1 values. Fourier transformation with respect to these two time domains generates a two-dimensional spectrum with two independent frequency dimensions, F_1 (from t_1) and F_2 (from t_2).

Most importantly, the signal eventually recorded during t_2 is modulated by events occurring during the evolution time t_1. As an example, consider a single isolated spin with a Larmor frequency Ω and a simple pulse sequence consisting of two 90°_x pulses separated by the variable period, t_1. Using the product operator formalism introduced in Chapter 2, the evolution of the density operator through the pulse sequence is

$$\begin{aligned} I_z &\xrightarrow{90^\circ_x} -I_y \\ &\xrightarrow{t_1} -I_y \cos(\Omega t_1) + I_x \sin(\Omega t_1) \\ &\xrightarrow{90^\circ_x} -I_z \cos(\Omega t_1) + I_x \sin(\Omega t_1) \\ &\xrightarrow{t_2} -I_z \cos(\Omega t_1) + I_x \sin(\Omega t_1) \cos(\Omega t_2) + I_y \sin(\Omega t_1) \sin(\Omega t_2) \end{aligned} \quad [4.1]$$

Thus, the complex signal detected during the acquisition period is proportional to $\sin(\Omega t_1) \exp(i\Omega t_2)$ and, as a result, depends parametrically upon the value of t_1. As shown in Fig. 4.3, following Fourier transformation of the data recorded during t_2, the amplitude of the resulting resonance signal depends on $\sin(\Omega t_1)$. A null signal is obtained if $\Omega t_1 = k\pi$, a signal with maximal amplitude is obtained if $\Omega t_1 = (4k+1)\pi/2$, and an inverted signal is obtained if $\Omega t_1 = (4k+3)\pi/2$, with k an integer. Formally, a *correlation* is established between the two time domains. The amplitude of the resonance signal obtained from the Fourier transformation of the data recorded during t_2, when displayed as a function of t_1, i.e., the data arrayed as a function of t_1 at a fixed value of F_2, forms an *interferogram* similar in appearance to the FID. The t_1 interferogram is indirectly sampled and differs in this respect

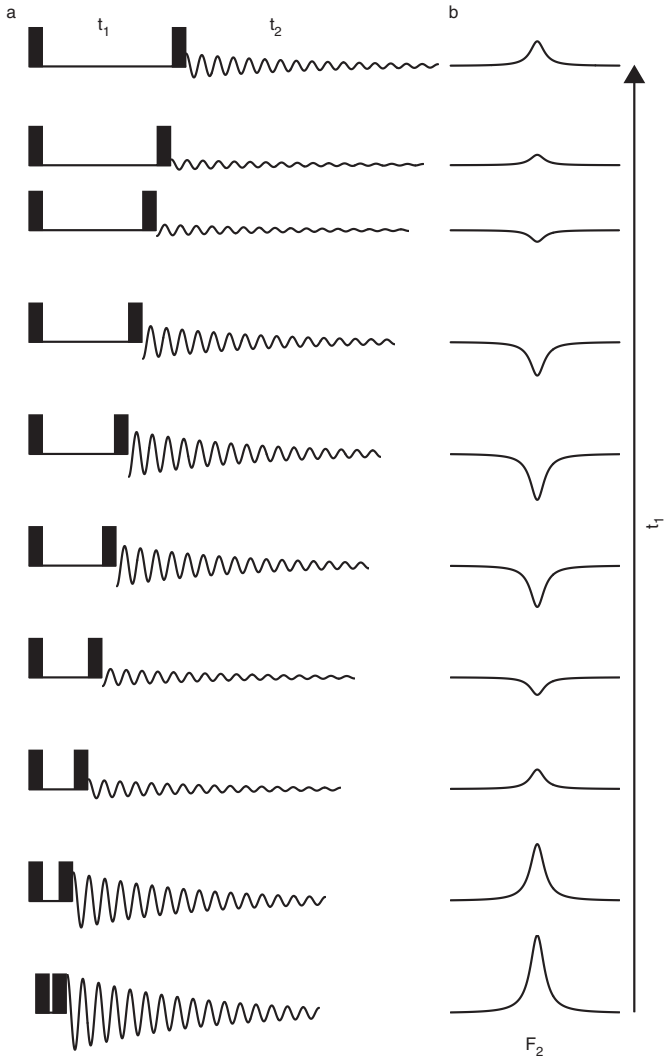

FIGURE 4.3 Dependence of the NMR signal on the evolution period, t_1. (a) The signal detected during the acquisition period, t_2, is modulated as a function of the evolution period, t_1. The vertical bars represent 90° pulses. The separation between the pulses is equal to t_1. (b) Following Fourier transformation of the recorded data with respect to t_2, the amplitude of the resonance signal varies periodically as a function of t_1 at a fixed value of F_2.

from the FID, which is directly detected by the spectrometer during t_2. Fourier transformation of the interferogram with respect to t_1 yields the F_1 dimension of the two-dimensional spectrum.

The correlation between the two time domains in the two-dimensional spectrum represented by [4.1] is trivial because the I spin operators precess at the same frequencies during t_1 and t_2 under the free-precession Hamiltonian. Consequently, signals are observed only at positions satisfying the relationship $F_1 = F_2$, and the conventional one-dimensional spectrum is reproduced along the diagonal of the two-dimensional spectrum. To provide additional information, a two-dimensional spectrum must contain resonance signals for which $F_1 \neq F_2$; this condition requires that the components of the density operator that eventually give rise to the observed resonance must evolve under different Hamiltonians during t_1 and t_2. Fortunately, because the components of the density operator that evolve during t_1 (or in fact any time before t_2) are never actually recorded, the mixing period can serve to transfer magnetization, or more generally, coherence, among spins prior to acquisition. The presence of a signal in the two-dimensional spectrum at one frequency in F_1 and at a second frequency in F_2 is direct evidence for transfer of coherence during the mixing period. With carefully constructed sequences of rf pulses and delays during the mixing period, correlations are established between the coherences present during t_1 and t_2 that result in chemically useful information.

To illustrate the importance of the mixing period, the example just discussed is extended to include a second spin, S, of the same nuclear species. The Larmor frequencies of the I and S spins are now designated Ω_I and Ω_S; the two spins are assumed to have a scalar coupling interaction with a coupling constant, J. Focusing on magnetization that originates on the I spin,

$$\begin{aligned}
I_z &\xrightarrow{90^\circ_x} -I_y \\
&\xrightarrow{t_1} -I_y \cos(\Omega_I t_1)\cos(\pi J t_1) + 2I_x S_z \cos(\Omega_I t_1)\sin(\pi J t_1) \\
&\qquad + I_x \sin(\Omega_I t_1)\cos(\pi J t_1) + 2I_y S_z \sin(\Omega_I t_1)\sin(\pi J t_1) \\
&\xrightarrow{90^\circ_x} -I_z \cos(\Omega_I t_1)\cos(\pi J t_1) - 2I_x S_y \cos(\Omega_I t_1)\sin(\pi J t_1) \\
&\qquad + I_x \sin(\Omega_I t_1)\cos(\pi J t_1) - 2I_z S_y \sin(\Omega_I t_1)\sin(\pi J t_1). \qquad [4.2]
\end{aligned}$$

Only the two terms proportional to I_x and $2I_zS_y$ on the last line of [4.2] result in detectable signals during the acquisition period. The first term leads to a detected signal proportional to $\sin(\Omega_I t_1)\cos(\pi J t_1)$

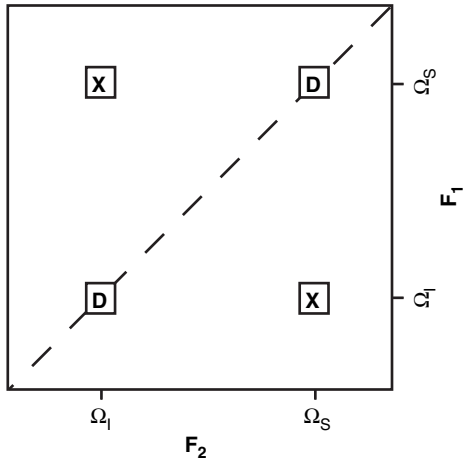

FIGURE 4.4 Schematic two-dimensional NMR spectrum for two spins, I and S. **D** represents diagonal peaks that occur at the same frequency in both dimensions and **X** represents cross-peaks that appear at different frequencies in each dimension. Cross-peaks result from the transfer of coherence from one spin to the other during the mixing period of the experiment. Diagonal peaks result from coherence that is not transferred between spins during the mixing period.

$\cos(\pi J t_2)\ \exp(i\Omega_I t_2)$; the second term leads to a signal proportional to $\sin(\Omega_I t_1)\ \sin(\pi J t_1)\ \sin(\pi J t_2)\ \exp(i\Omega_S t_2)$. A complementary coherence transfer pathway also exists, whereby magnetization originating on the S spin is transferred to the I spin during the mixing period. This complementary pathway leads to detectable signals proportional to $\sin(\Omega_S t_1)\ \cos(\pi J t_1)\ \cos(\pi J t_2)\ \exp(i\Omega_S t_2)$ and $\sin(\Omega_S t_1)\ \sin(\pi J t_1)\ \sin(\pi J t_2)\ \exp(i\Omega_I t_2)$. Ignoring multiplet structures and peak shapes for the present discussion (see Section 6.2.1), Fourier transformation with respect to t_1 and t_2 generates a (schematic) spectrum of the form shown in Fig. 4.4. Two peaks, **D**, known as *diagonal peaks*, are observed at frequencies $(F_1,\ F_2) = (\Omega_I,\ \Omega_I)$ and $(F_1,\ F_2) = (\Omega_S,\ \Omega_S)$. The diagonal peaks result from magnetization that remains on the same spin I or S throughout the experiment and essentially form a one-dimensional spectrum. On the other hand, the two peaks, **X**, known as *cross-peaks*, result from magnetization that has been transferred from one spin to the other during the mixing period. Inspection of [4.2] shows that the cross-peak at $(F_1,\ F_2) = (\Omega_I,\ \Omega_S)$ results from the $2I_zS_y$ operator present at the beginning of t_2. This operator is

generated by the second 90°_x pulse in the sequence acting on the $2I_yS_z$ operator. The action of this pulse results in the conversion of an antiphase I operator, which evolves with Larmor frequency Ω_I during t_1, into an antiphase S operator, which evolves with Larmor frequency Ω_S during t_2; thereby, coherence is transferred from the I spin to the S spin. The cross-peak at $(F_1, F_2) = (\Omega_S, \Omega_I)$ results from the complementary transfer of coherence from the S spin to the I spin. The second pulse in this experiment comprises the entire mixing period.

In the present case, the mixing sequence was designed to effect transfer of magnetization via the scalar coupling between two spins; consequently, the appearance of cross-peaks between spins I and S in the spectrum unambiguously indicates that the two spins are scalar coupled and establishes a through-bond correlation between the spins. In fact, this *gedanken* experiment is the basis of the original two-dimensional NMR technique, the COSY (correlated spectroscopy) experiment, discussed in Section 6.2 (*8–10*). Detection of a scalar coupling interaction between the two spins does not depend upon observation of changes in the multiplet structure or intensity of the diagonal resonances as in one-dimensional NMR experiments, but rather upon the appearance of cross-peaks in the two-dimensional spectrum. This property gives multidimensional spectroscopy its immense power: not only are important correlations established, but the two independent frequency coordinates effectively increase the resolution in the spectrum. Overlapping signals in the conventional one-dimensional spectrum, which arise, for example, from multiple scalar coupling interactions, are dispersed into the additional frequency dimension in a process called *separation of interactions*.

The frequency in the F_2 dimension (recorded during t_2) of each peak in the two-dimensional spectrum must correspond to the frequency of a peak in the conventional one-dimensional spectrum. The converse is not true, because certain resonances in the one-dimensional spectrum can be suppressed in the two-dimensional spectrum. Removal of undesirable resonances by using multiple-quantum and isotope filters are discussed in Chapters 6, 7, and 9. The F_1 frequency of a peak in the two-dimensional spectrum need not correspond to a frequency in the conventional spectrum; the exact form of the relationship between the F_1 and F_2 frequencies of a peak in the two-dimensional spectrum will depend on the particular manipulations of the spins before acquisition. Two very useful features arise because the evolution of a coherence during t_1 is never actually physically detected. First, the coherence that is present during t_1 can be of a type that cannot

normally be recorded, such as multiple-quantum coherence. A typical experiment of this kind would proceed by preparing multiple-quantum coherence, frequency labeling the coherence during t_1, and returning the multiple-quantum coherence to single-quantum coherence for detection. Second, the frequencies of peaks in F_1 can be manipulated to be different from the actual frequencies with which coherences evolve during t_1. Examples of this type of experiment include the removal of chemical shift evolution and heteronuclear scalar couplings by the application of a 180° pulse at the midpoint of t_1.

The functions of the different periods of a two-dimensional NMR experiment are summarized as follows:

1. *Preparation*: The desired nonequilibrium state of the spin system is prepared from the initial (equilibrium) state of the spin system. The preparation period in its simplest form consists of a single pulse that generates transverse magnetization, but more complex sequences of pulses can be used to prepare other coherences, such as multiple quantum coherences, and to perform solvent suppression.
2. *Evolution*: The off-diagonal components of the density operator prepared in step (1) evolve under the Hamiltonian, $\mathscr{H}_e$. During the course of the experiment, the incrementable time t_1 normally begins at an initial value and increases in discrete steps to a maximum value, $t_{1\max}$. The Hamiltonian, $\mathscr{H}_e$, may be the free-precession Hamiltonian or may include applied rf fields. The frequencies with which the detected coherence evolves during t_1 results in signals appearing at those frequencies in the F_1 dimension of the final two-dimensional spectrum. This process is known as F_1 frequency labeling of the coherence.
3. *Mixing*: During the mixing period, coherence is transferred from one spin to another. The mixing period is the key to establishing the type of correlation between the two dimensions and consequently dictates the information content of the spectrum. Depending on the type of experiment, the mixing period consists of one or more pulses and delays.
4. *Acquisition*: The FID is recorded in the conventional fashion. As discussed in Section 4.3, if more than one coherence transfer pathway is feasible, phase cycling or field gradient pulses are used to determine which coherence transfer processes contribute to the final spectrum.

The evolution of the density operator of the spin system during the pulse sequence is described, using the product operator formalism, as a transformation of the density operator from its initial to final value

during each of the four parts of the experiment. Thus,

$$\begin{aligned}
\sigma^{\text{eq}} &\xrightarrow{\text{Preparation}} \sigma(0), \\
\sigma(0) &\xrightarrow{\text{Evolution}} \sigma(t_1), \\
\sigma(t_1) &\xrightarrow{\text{Mixing}} \sigma(t_1, 0), \\
\sigma(t_1, 0) &\xrightarrow{\text{Acquisition}} \sigma(t_1, t_2).
\end{aligned} \qquad [4.3]$$

The modular nature of two-dimensional NMR experiments evident from this discussion facilitates the construction of new experiments from combinations of prefabricated "building-block" pulse sequences that effect particular transformations of the density operator. This approach is even more powerful for the design of three- and four-dimensional experiments, as will be discussed in subsequent chapters.

4.2 Coherence Transfer and Mixing

The key to obtaining useful chemical or structural information from two-dimensional NMR spectroscopy is the transfer of coherence from one spin to another during the mixing period. In the following sections, two mechanisms for transferring coherence between spins in multidimensional NMR spectroscopy are discussed. Coherence transfer in homonuclear spin systems is discussed first; the generalization to heteronuclear spin systems follows directly. This presentation is not meant to represent a comprehensive account of magnetization transfer processes in multidimensional spectroscopy. Rather, the idea that *through-bond* scalar coupling and *through-space* dipolar interactions are responsible for transfer of coherence between spins should be appreciated.

4.2.1 THROUGH-BOND COHERENCE TRANSFER

A crucial mixing process in many multidimensional experiments is migration of coherence among scalar-coupled nuclei. This process, known as coherence transfer, has already been introduced in Section 2.7.6. Coherence transfer can be produced by evolution of the spin system under a series of rf pulses and free-precession delays ("pulse-interrupted free precession" or COSY-type coherence transfer), or by cross-polarization of the spin system by using continuous, time-varying rf fields [TOCSY-type or homonuclear Hartmann–Hahn

(HOHAHA)-type coherence transfer]. Scalar coupling interactions are mediated by covalent bonding interactions; therefore, COSY and TOCSY mixing generate through-bond coherence transfer.

4.2.1.1 COSY-Type Coherence Transfer The density operator must contain antiphase terms in order to transfer coherence from one spin to another by COSY techniques (*8, 9*). Thus, before coherence transfer can be achieved, antiphase coherence must develop from in-phase coherence by evolution under the scalar coupling interaction between spins. The antiphase coherence with respect to one spin is transferred by the mixing pulse into antiphase coherence with respect to the scalar-coupled partner. This coherence transfer process is illuminated by considering the effect of the pulse sequence,

$$90^\circ_x\text{–}\tau/2\text{–}180^\circ_y\text{–}\tau/2\text{–}90^\circ_y, \qquad [4.4]$$

on a weakly coupled homonuclear *IS* spin system, with a mutual scalar coupling constant J_{IS}. Using [2.121], the propagator for the pulse sequence is

$$\mathbf{U} = \exp\left[i\tfrac{\pi}{2}(I_y + S_y)\right] \exp[-i2\pi J_{IS}\tau I_z S_z] \exp\left[-i\tfrac{\pi}{2}(I_x + S_x)\right]. \qquad [4.5]$$

As discussed in Section 2.7.7.1, the 180° pulse refocuses chemical shift evolution; in addition, this pulse effectively inverts the phase of the second 90° pulse. The principles of the experiment are deduced by concentrating on the fate of just one of the spins. Starting with equilibrium I spin magnetization, I_z, the analysis proceeds as follows:

$$\begin{aligned} I_z &\xrightarrow{90^\circ_x} -I_y \\ &\xrightarrow{\tau} -I_y \cos(\pi J_{IS}\tau) + 2I_x S_z \sin(\pi J_{IS}\tau) \\ &\xrightarrow{90^\circ_{-y}} -I_y \cos(\pi J_{IS}\tau) - 2I_z S_x \sin(\pi J_{IS}\tau). \end{aligned} \qquad [4.6]$$

The term proportional to I_y represents coherence of spin I that is not transferred to spin S during the sequence. The term $2I_zS_x$ corresponds to antiphase single-quantum coherence of the S spin and represents coherence transferred to the S spin from the I spin by the mixing sequence. Notice that the $2I_zS_x$ operator was generated by the application of the 90°_y pulse to the antiphase operator $2I_xS_z$. Of course, the analogous treatment for the S spin results in transfer of coherence from the S spin to the I spin during the mixing sequence. The coefficients of the operators depend upon the rate at which the antiphase coherence evolves. The amount of coherence passed from one spin to a

scalar-coupled partner is termed the *coherence transfer amplitude*. In the present example, the coherence transfer amplitude is given by $\sin(\pi J_{IS}\tau)$, and is maximal when $\tau = 1/(2J_{IS})$. As stated previously, for coherence transfer to proceed at all, the system must have evolved to an antiphase state with respect to the scalar coupling during the period τ.

Now consider the extension to the situation in which spin I is coupled to two other spins, R and S, with scalar coupling constants J_{IR} and J_{IS}. The R and S spins are assumed to lack a scalar coupling interaction (i.e., $J_{RS} = 0$). The product operator analysis of the mixing sequence yields

$$\begin{aligned}
I_z &\overset{90^\circ_x}{\rightarrow} -I_y \\
&\overset{\tau}{\rightarrow} -I_y \cos(\pi J_{IR}\tau)\cos(\pi J_{IS}\tau) + 2I_xR_z \sin(\pi J_{IR}\tau)\cos(\pi J_{IS}\tau) \\
&\qquad + 2I_xS_z \cos(\pi J_{IR}\tau)\sin(\pi J_{IS}\tau) + 4I_yR_zS_z \sin(\pi J_{IR}\tau)\sin(\pi J_{IS}\tau) \\
&\overset{90^\circ_{-y}}{\rightarrow} -I_y \cos(\pi J_{IR}\tau)\cos(\pi J_{IS}\tau) - 2I_zR_x \sin(\pi J_{IR}\tau)\cos(\pi J_{IS}\tau) \\
&\qquad - 2I_zS_x \cos(\pi J_{IR}\tau)\sin(\pi J_{IS}\tau) + 4I_yR_xS_x \sin(\pi J_{IR}\tau)\sin(\pi J_{IS}\tau).
\end{aligned} \qquad [4.7]$$

Again, the term proportional to I_y represents coherence of spin I that is not transferred to either coupled spin during the sequence. The term $2I_zR_x$ corresponds to antiphase single-quantum coherence of the R spin and represents coherence transferred to the R spin from the I spin by the mixing sequence. Similarly, the term $2I_zS_x$ corresponds to antiphase single-quantum coherence of the S spin and represents coherence transferred to the S spin from the I spin by the mixing sequence. The term $4I_yR_xS_x$ represents a linear combination of multiple-quantum coherences and is not of further interest here (but see Section 6.4.2). Analogous treatments for the R and S spins result in transfers of coherence from the R and S spins to the I spin. No coherence is transferred between spins R and S because they are not scalar coupled to each other, even though they are mutually coupled to the I spin.

In the present example, the I spin evolves under the influence of two scalar coupling interactions during τ. In the evolution leading to the term $2I_xR_z$, the scalar coupling to spin R is called the active coupling and the scalar coupling to spin S is called the passive coupling; in the evolution leading to the term $2I_xS_z$, the scalar coupling to spin R is called the passive coupling and the scalar coupling to spin S is called the active coupling. As shown, each active coupling contributes a factor of

$\sin(\pi J_a \tau)$, in which J_a is the active scalar coupling constant, and each passive coupling contributes a factor of $\cos(\pi J_p \tau)$, in which J_p is the passive scalar coupling constant, to the magnitude of the product operators. If a given spin is scalar coupled to N other spins, the operators that lead to coherence transfer in the COSY-type mixing sequences have a single active coupling and $N-1$ passive couplings; operators with no active couplings represent operators for which no coherence transfer occurs, and operators with greater than one active coupling represent the creation of multiple-quantum coherences. As before, the coefficients of the operators depend upon the rate at which antiphase coherence is generated. However, to maximize coherence transfer from I to R or S requires knowledge of the values of J_{IR} and J_{IS}. In general, coherence transfers from I to R and from I to S are not maximized for the same value of τ unless $J_{IR} = J_{IS}$. In addition, coherence transfer efficiencies cannot be simultaneously maximized for two and three (or more) spin systems because of the different trigonometric expressions encountered in [4.6] and [4.7].

The final operator of interest in [4.6] is an antiphase S operator. In some circumstances, coherence transfer to an in-phase operator is desirable. In the COSY-style mixing sequences, a second delay period must be used to refocus the antiphase operator. The entire mixing sequence is

$$90^\circ_x\text{–}\tau/2\text{–}180^\circ_y\text{–}\tau/2\text{–}90^\circ_y\text{–}\tau_2/2\text{–}180^\circ_y\text{–}\tau_2/2. \qquad [4.8]$$

By the same reasoning as for [4.4] and [4.5], the effects of the pulse sequence are obtained by analysis of the propagator:

$$\begin{aligned}\mathbf{U} = {} & \exp[-i2\pi J_{IS}\tau_2 I_z S_z]\ \exp\left[i\tfrac{\pi}{2}(I_y + S_y)\right] \\ & \times \exp[-i2\pi J_{IS}\tau I_z S_z]\ \exp\left[-i\tfrac{\pi}{2}(I_x + S_x)\right], \end{aligned} \qquad [4.9]$$

in which only the scalar coupling Hamiltonian is effective during τ and τ_2. The evolution up to the 90°_y pulse has already been presented in [4.6] and [4.7]; only the analysis of the additional effects of the τ_2 period must be considered here. For simplicity, only the antiphase term $2I_zS_x$, which results from the coherence transfer step analyzed in [4.6], is treated:

$$\begin{aligned} 2I_zS_x \sin(\pi J_{IS}\tau) \xrightarrow{\tau_2} {} & 2I_zS_x \sin(\pi J_{IS}\tau)\cos(\pi J_{IS}\tau_2) \\ & + S_y \sin(\pi J_{IS}\tau)\sin(\pi J_{IS}\tau_2). \end{aligned} \qquad [4.10]$$

The second term on the right-hand side of [4.10] represents in-phase transverse magnetization of the S spin. Complete refocusing of the

antiphase operator is obtained for $\tau_2 = 1/(2J_{IS})$. Thus, coherence transfer from an in-phase state on one spin to an in-phase state on a coupled spin requires a total time of $1/J_{IS}$ when employing pulse-interrupted free-precession methods.

The principal limitation of COSY-type coherence transfer arises from the antiphase multiplet structure of the resulting cross-peaks in the spectrum. If the size of the active coupling is comparable to the linewidth, partial cancellation of the multiplet occurs due to destructive interference between the antiphase components of the peak. To avoid self-cancellation, the antiphase components must be refocused, so that the resulting cross-peak multiplet is composed of peaks entirely of the same algebraic sign. The destructive interference effects are then eliminated, but only at the expense of an additional refocusing period of duration $1/(2J_{IS})$. A more detailed discussion of COSY experiments is given in Section 6.2.

4.2.1.2 TOCSY Transfer Through-Bonds Thus far, coherence transfer has been limited to pulse-interrupted free-precession techniques, or COSY-type transfer via evolution under the scalar coupling Hamiltonian in the weak coupling limit. To begin the present discussion, consider the evolution of the density operator under the strong scalar coupling Hamiltonian between two spins I and S (*11*):

$$\mathscr{H} = 2\pi J_{IS}\,\mathbf{I}\cdot\mathbf{S} = 2\pi J_{IS}\big(I_xS_x + I_yS_y + I_zS_z\big). \qquad [4.11]$$

The evolution of the I_z operator is given by

$$\begin{aligned}
&\exp(-i\mathscr{H}\tau_{\mathrm{m}})I_z\exp(i\mathscr{H}\tau_{\mathrm{m}})\\
&\quad=\exp\big[-i2\pi J_{IS}\tau_{\mathrm{m}}\big(I_xS_x+I_yS_y+I_zS_z\big)\big]I_z\\
&\qquad\times\exp\big[i2\pi J_{IS}\tau_{\mathrm{m}}\big(I_xS_x+I_yS_y+I_zS_z\big)\big]\\
&\quad=\exp(-i\zeta 2I_xS_x)\exp\big(-i\zeta 2I_yS_y\big)\exp(-i\zeta 2I_zS_z)I_z\\
&\qquad\times\exp(i\zeta 2I_zS_z)\exp\big(i\zeta 2I_yS_y\big)\exp(i\zeta 2I_xS_x)\\
&\quad=\exp(-i\zeta 2I_xS_x)\exp\big(-i\zeta 2I_yS_y\big)I_z\exp\big(i\zeta 2I_yS_y\big)\exp(i\zeta 2I_xS_x),
\end{aligned} \qquad [4.12]$$

in which $\zeta = \pi J_{IS}\tau_{\mathrm{m}}$, τ_{m} is the mixing time, and the third line is obtained because the operators I_xS_x, I_yS_y, and I_zS_z commute with each other. The evolution is calculated by making use of [2.121] to evaluate the effects of

the propagator $\mathbf{U} = \exp(-i\zeta I_y S_y)$,

$$\begin{aligned}
&\exp\left(-i\zeta 2I_y S_y\right) I_z \exp\left(i\zeta 2I_y S_y\right) \\
&\quad = \exp\left(-i\tfrac{\pi}{2}I_x\right) \exp\left(-i\tfrac{\pi}{2}S_x\right) \exp(-i\zeta 2I_z S_z) \exp\left(i\tfrac{\pi}{2}S_x\right) \exp\left(i\tfrac{\pi}{2}I_x\right) I_z \\
&\qquad \times \exp\left(-i\tfrac{\pi}{2}I_x\right) \exp\left(-i\tfrac{\pi}{2}S_x\right) \exp(i\zeta 2I_z S_z) \exp\left(i\tfrac{\pi}{2}S_x\right) \exp\left(i\tfrac{\pi}{2}I_x\right) \\
&\quad = \exp\left(-i\tfrac{\pi}{2}I_x\right) \exp\left(-i\tfrac{\pi}{2}S_x\right) \exp(-i\zeta 2I_z S_z) I_y \exp(i\zeta 2I_z S_z) \\
&\qquad \times \exp\left(i\tfrac{\pi}{2}S_x\right) \exp\left(i\tfrac{\pi}{2}I_x\right) \\
&\quad = \exp\left(-i\tfrac{\pi}{2}I_x\right) \exp\left(-i\tfrac{\pi}{2}S_x\right)\left(I_y \cos\zeta - 2I_x S_z \sin\zeta\right) \exp\left(i\tfrac{\pi}{2}S_x\right) \exp\left(i\tfrac{\pi}{2}I_x\right) \\
&\quad = \exp\left(-i\tfrac{\pi}{2}I_x\right)\left(I_y \cos\zeta + 2I_x S_y \sin\zeta\right) \exp\left(i\tfrac{\pi}{2}I_x\right) \\
&\quad = I_z \cos\zeta + 2I_x S_y \sin\zeta,
\end{aligned} \tag{4.13}$$

followed by $\mathbf{U} = \exp(-i\zeta I_x S_x)$,

$$\begin{aligned}
&\exp(-i\zeta 2I_x S_x)\left(I_z \cos\zeta + 2I_x S_y \sin\zeta\right) \exp(i\zeta 2I_x S_x) \\
&\quad = \exp\left(-i\tfrac{\pi}{2}I_y\right) \exp\left(-i\tfrac{\pi}{2}S_y\right) \exp(-i\zeta 2I_z S_z) \exp\left(i\tfrac{\pi}{2}S_y\right) \exp\left(i\tfrac{\pi}{2}I_y\right) \\
&\qquad \times \left(I_z \cos\zeta + 2I_x S_y \sin\zeta\right) \\
&\qquad \times \exp\left(-i\tfrac{\pi}{2}I_y\right) \exp\left(-i\tfrac{\pi}{2}S_y\right) \exp(i\zeta 2I_z S_z) \exp\left(i\tfrac{\pi}{2}S_y\right) \exp\left(i\tfrac{\pi}{2}I_y\right) \\
&\quad = I_z \cos^2\zeta + \left(-2I_y S_x + 2I_x S_y\right) \cos\zeta \sin\zeta + S_z \sin^2\zeta,
\end{aligned} \tag{4.14}$$

to yield the final result,

$$\begin{aligned}
I_z &\xrightarrow{\mathscr{H}\tau_m} I_z \cos^2(\pi J_{IS}\tau_m) + S_z \sin^2(\pi J_{IS}\tau_m) \\
&\qquad + 2\left(I_x S_y - I_y S_x\right) \cos(\pi J_{IS}\tau_m) \sin(\pi J_{IS}\tau_m), \\
S_z &\xrightarrow{\mathscr{H}\tau_m} I_z \sin^2(\pi J_{IS}\tau_m) + S_z \cos^2(\pi J_{IS}\tau_m) \\
&\qquad - 2\left(I_x S_y - I_y S_x\right) \cos(\pi J_{IS}\tau_m) \sin(\pi J_{IS}\tau_m),
\end{aligned} \tag{4.15}$$

in which the evolution of the S_z operator is obtained by exchanging the I and S labels. Equation [4.15] predicts that the sum, $I_z + S_z$, is a constant and that the difference, $I_z - S_z$, is given by

$$(I_z - S_z) \xrightarrow{\mathscr{H}\tau_m} (I_z - S_z) \cos(2\pi J_{IS}\tau_m) + 2(I_x S_y - I_y S_x) \sin(2\pi J_{IS}\tau_m). \tag{4.16}$$

If $\tau_m = 1/(2J_{IS})$, I_z magnetization is transferred completely to S_z magnetization and *vice versa*. Evolution under the strong coupling Hamiltonian transfers in-phase magnetization between spins in a time of $1/(2J_{IS})$, compared with the time of $1/J_{IS}$ required for in-phase coherence

transfer in weakly coupled systems via free-precession techniques. In addition, in a three-spin *IRS* system, magnetization can be transferred from R to S even if $J_{RS}=0$ by the two-step transfer $R_z \rightarrow I_z \rightarrow S_z$.

In real situations, the Hamiltonian for a spin system contains chemical shift and rf terms in addition to the scalar coupling interaction. Magnetization transfer via the strong scalar coupling interaction is efficient only if all chemical shift and rf terms of the Hamiltonian governing the spin system have identical values for each of the two spins I and S. This is the *Hartmann–Hahn* condition (*12*). Coherence transfer via Hartmann–Hahn cross-polarization has been used extensively in heteronuclear NMR experiments in the solid state. Braunschweiler and Ernst first demonstrated the feasibility of Hartmann–Hahn cross-polarization in homonuclear solution-phase NMR spectroscopy (*11*).

Hartmann–Hahn matching in the rotating reference frame can be achieved by application of an rf field of sufficient strength that any offset and chemical shift effects are negligible in comparison. Müller and Ernst (*13*) demonstrated that transfer of I spin magnetization to the S spin, keeping only the in-phase operators of interest, proceeds as,

$$\begin{aligned} I_z &\xrightarrow{\mathscr{H}\tau_m} I_z a_{II}(\tau_m) + S_z a_{IS}(\tau_m), \\ S_z &\xrightarrow{\mathscr{H}\tau_m} I_z a_{SI}(\tau_m) + S_z a_{SS}(\tau_m), \end{aligned} \qquad [4.17]$$

in which

$$\begin{aligned} a_{II}(\tau_m) &= 1 - \sin^2\phi \, \sin^2(q\tau_m), \\ a_{SS}(\tau_m) &= 1 - \sin^2\phi \, \sin^2(q\tau_m), \\ a_{IS}(\tau_m) &= a_{SI}(\tau_m) = \sin^2\phi \, \sin^2(q\tau_m), \end{aligned} \qquad [4.18]$$

and

$$\begin{aligned} q &= \left((\Omega_{I(\text{eff})} - \Omega_{S(\text{eff})})^2 + (\pi J_{IS} \, \sin\theta_I \, \sin\theta_S)^2\right)^{1/2}, \\ \tan\phi &= \frac{1}{2}\left(\frac{2\pi J_{IS} \, \sin\theta_I \, \sin\theta_S}{\Omega_{I(\text{eff})} - \Omega_{S(\text{eff})}}\right), \\ \Omega_{I(\text{eff})} &= \left[\Omega_I^2 + \omega_{1I}^2\right]^{1/2} \quad \text{and} \quad \Omega_{S(\text{eff})} = \left[\Omega_S^2 + \omega_{1S}^2\right]^{1/2}, \\ \theta_I &= \tan^{-1}\left(\frac{\omega_{1I}}{\Omega_I}\right) \quad \text{and} \quad \theta_S = \tan^{-1}\left(\frac{\omega_{1S}}{\Omega_S}\right). \end{aligned} \qquad [4.19]$$

Here θ_I and θ_S are the tilt angles of the effective field at the I and S spins, respectively, ω_{1I} and ω_{1S} are the rf field strengths experienced by the I and S spins, respectively; Ω_I is the I spin offset, Ω_S is the S spin offset, and J_{IS} is the scalar coupling constant between the I and S spins.

In [4.17], $a_{II}(\tau_m)$ is the amount of magnetization remaining on spin I, $a_{SS}(\tau_m)$ is the amount of magnetization remaining on spin S, and $a_{IS}(\tau_m)$ is the amount of magnetization transferred to spin S at time τ_m. The functions $a_{II}(\tau_m)$, $a_{SS}(\tau_m)$, and $a_{IS}(\tau_m)$ frequently are called the mixing coefficients. If $\Omega_I = \pm\Omega_S$, then the Hartmann–Hahn matching condition is satisfied because $\Omega_{I(\text{eff})} = \Omega_{S(\text{eff})}$. For the special case $\Omega_I = \Omega_S = 0$, [4.17] reduces to [4.15]. If the two scalar-coupled spins have different offsets from the rf carrier frequency, $|\Omega_I| \neq |\Omega_S|$, Hartmann–Hahn matching becomes more difficult, and magnetization transfer is reduced drastically. In practice, the power required to accomplish efficient Hartmann–Hahn matching over a significant frequency range $\Omega_I \neq |\Omega_S|$ by using a continuous rf field would produce disastrous sample and probe heating effects.

As shown by [4.17], differences in chemical shift between two coupled spins prevent efficient Hartmann–Hahn matching by application of a continuous rf field. Ideally, an effective Hamiltonian is required such that it eliminates the chemical shift terms over a significant frequency range while the rf field is applied. In effect, the spin Hamiltonian, $\mathscr{H}$, must be reduced from

$$\mathscr{H} = \sum_i -\omega_i I_{iz} + 2\pi \sum_{i \neq j} J_{ij} \mathbf{I}_i \cdot \mathbf{I}_j \qquad [4.20]$$

to an effective Hamiltonian,

$$\mathscr{H} = 2\pi \sum_{i \neq j} J_{ij} \mathbf{I}_i \cdot \mathbf{I}_j \qquad [4.21]$$

for a period τ_m, which is of the order of $1/J_{ij}$ (*11*). The last equation consists of just the pure scalar coupling term, in which all shift terms or linear operators are removed, leaving only bilinear operators. The absence of chemical shift terms means that the Hartmann–Hahn condition is always satisfied. A pulse sequence that generates an average Hamiltonian given by [4.21] is said to be *isotropic*. Magnetization transfer under the influence of such a sequence is a continuous mixing process, with the magnetization moving in a periodic fashion among all the spins in the scalar-coupled network. Such pulse sequences shall be referred to as *isotropic mixing sequences*. An important practical consequence of an isotropic mixing sequence is that the transfer of magnetization occurs equally well for all angular momentum components. That is, coherent exchange of difference magnetization will occur under the isotropic scalar coupling Hamiltonian according to [4.16] with

similar relations for the x and y components, obtained by cyclic permutation of the indices:

$$(I_x - S_x) \xrightarrow{\mathscr{H}\tau_m} (I_x - S_x)\cos(2\pi J_{IS}\tau_m) + (I_yS_z - I_zS_y)\sin(2\pi J_{IS}\tau_m), \quad [4.22]$$

$$(I_y - S_y) \xrightarrow{\mathscr{H}\tau_m} (I_y - S_y)\cos(2\pi J_{IS}\tau_m) + (I_xS_z - I_zS_x)\sin(2\pi J_{IS}\tau_m). \quad [4.23]$$

The design and performance properties of experimental techniques to achieve isotropic mixing are described in Section 6.5.

Until now, the second terms on the right-hand sides of [4.16], [4.22], and [4.23] have not been considered. These terms contain bilinear product operators that are orthogonal to the in-phase terms of interest. The bilinear term in [4.16] is a multiple-quantum coherence term, while bilinear terms in [4.22] and [4.23] represent antiphase single-quantum coherence operators. The significance of the bilinear terms will be discussed for [4.22], although the arguments are applicable equally to the other cases. Simple inspection shows that the antiphase term has y-phase while the in-phase term has x-phase; thus a 90° phase difference exists between the terms. If the signal resulting from the in-phase magnetization is phased to be absorptive, then the signal resulting from the antiphase term automatically becomes dispersive. The dispersive antiphase multiplets occur in the same spectral position in which the in-phase absorptive peaks occur, and can disrupt the lineshapes in the two-dimensional NMR spectrum. Indeed, for small molecules with narrow linewidths, interference from the dispersive antiphase components can be observed. In contrast, the resonance peaks for large biological macromolecules usually appear to be completely absorptive, because the linewidths are notably larger, and the dispersive antiphase components self-cancel very efficiently. Dispersive antiphase resonances can be suppressed further by z-filtration (Section 6.5) (*14, 15*).

To summarize, coherence transfer is obtained when two scalar-coupled spins are subjected simultaneously to an rf field that effectively removes the chemical shifts of the spins. When used for homonuclear coherence transfer under the scalar coupling Hamiltonian, this technique often is referred to as a homonuclear Hartmann–Hahn (*16*) experiment to indicate the required Hartmann–Hahn matching condition. Throughout the remainder of this text, isotropic mixing sequences that satisfy the Hartmann–Hahn condition will be used to mediate coherence transfer. Pulse sequences utilizing isotropic mixing will be

referred to as TOCSY (total correlation spectroscopy) experiments, as originally suggested by Braunschweiler and Ernst (*11*). The use of the word "total" in deriving the acronym implies that all spins belonging to a scalar-coupled network are connected by such an experiment.

4.2.2 THROUGH-SPACE COHERENCE TRANSFER

As will be discussed in Sections 5.1.2 and 5.5, perturbing the populations of stationary states within a spin system causes time-dependent changes in the intensities of dipolar-coupled resonance signals via the NOE (nuclear Overhauser effect) (*3, 4*). Dipolar cross-relaxation is an extremely useful mixing process in multidimensional NMR spectroscopy, because the efficiency of mixing depends upon the distance between interacting spins. Thus, *through-space*, rather than *through-bond*, magnetization transfer generates cross-peaks in the NOE mixing process.

Consider the effect of the following pulse sequence on a pair of dipolar coupled spins, I and S, which have no scalar coupling between them:

$$90^\circ_x\text{–}t_1\text{–}90^\circ_x\text{–}\tau_m\text{–}90^\circ_x\text{–}t_2. \qquad [4.24]$$

This pulse sequence is known as the NOESY (nuclear Overhauser enhancement spectroscopy) (*17*) experiment and is the most powerful and important technique available for structural investigations of biomolecules by solution-state NMR spectroscopy. A more detailed account of this experiment will be presented in Section 6.6.1. Concentrating solely on the I spin, the following product operators are present after the second 90°_x pulse:

$$I_z \xrightarrow{(\pi/2)_x - t_1 - (\pi/2)_x} -I_z \cos(\Omega_I t_1) + I_x \sin(\Omega_I t_1). \qquad [4.25]$$

Experimentally the I_x term is suppressed by phase cycling or by application of a field gradient pulse (Section 4.3), which leaves only the $-I_z \cos(\Omega_I t_1)$ term. A close analogy to the one-dimensional transient NOE experiment (Section 5.1.2) now is apparent. The term $-I_z \cos(\Omega_I t_1)$ represents a perturbation of the I spin from the equilibrium $+I_z$ state. The perturbation depends upon the value of t_1; for example, whenever $\Omega_I t_1 = 2\pi$, the populations are inverted across the I spin transitions. Consequently an NOE will be induced on the S spin during the fixed delay, τ_m, because the I and S spins have a dipolar coupling. The delay, τ_m, is known as the mixing time and is set to a suitable value (of the

order of $\leq 1/R_1$) to allow a significant NOE to develop. The effect of cross-relaxation during the mixing time is represented as:

$$-I_z \cos(\Omega_I t_1) \xrightarrow{\tau_m} -I_z \cos(\Omega_I t_1) a_{II}(\tau_m) - S_z \cos(\Omega_I t_1) a_{IS}(\tau_m), \quad [4.26]$$

in which $a_{II}(\tau_m)$ represents the fraction of the original magnetization remaining on the I spin, and $a_{IS}(\tau_m)$ represents the fraction of the original magnetization transferred from the I spin to the S spin during the mixing time by dipolar cross relaxation. The functional forms of $a_{II}(\tau_m)$ and $a_{IS}(\tau_m)$ are discussed more fully in Section 5.1.2. The final pulse generates an observable term on the S spin of the form $S_y \cos(\Omega_I t_1) a_{IS}(\tau_m)$; upon two-dimensional Fourier transformation, a cross-peak will be generated at frequency $(F_1, F_2) = (\Omega_I, \Omega_S)$ with amplitude proportional to $a_{IS}(\tau_m)$. For any magnetization that remains on the I spin, the final pulse will result in an observable term of the form $I_y \cos(\Omega_I t_1) a_{II}(\tau_m)$, which will yield a diagonal peak with frequency coordinates of $(F_1, F_2) = (\Omega_I, \Omega_I)$. Identical pathways also exist for magnetization transfer S to I and corresponding diagonal and cross-peaks result.

4.2.3 HETERONUCLEAR COHERENCE TRANSFER

In multidimensional NMR spectroscopy, different spins in a molecule are correlated by separating their interactions into more than one frequency dimension; however, the interacting spins do not necessarily have to be of the same nuclear species. Coherence can be transferred between different nuclear species using techniques analogous to those presented for homonuclear spin systems. The corollaries to the COSY-style homonuclear coherence transfer sequences are the INEPT (*18, 19*) and distortionless enhancement by polarization transfer (DEPT) (*20, 21*) family of pulse sequences. Heteronuclear cross-polarization corresponds to the TOCSY-style homonuclear sequences. Heteronuclear NOESY magnetization transfer via the heteronuclear dipolar coupling is analogous to the homonuclear experiment (*22, 23*). In heteronuclear experiments, rf pulses are applied at more than one frequency (typically differing by hundreds of megahertz) in order to manipulate both the heteronuclear and the ^{1}H spins. Thus, in contrast to homonuclear experiments in which nonselective pulses affect all nuclei, different nuclear species are manipulated independently by rf pulses. As has already been shown in Section 2.7.7.2, the product operator approach can be used to describe manipulations of spin systems that

contain operators corresponding to different nuclear species. As will be seen in Chapter 7, some of the most powerful multidimensional NMR methods rely on heteronuclear coherence transfer between $^{13}C/^{15}N$ and ^{1}H.

4.2.4 Coherence Transfer under Residual Dipolar Coupling Hamiltonians

As described in Section 2.8, in an anisotropic environment, induced by external fields or physical media such as liquid crystalline materials, the direct dipole–dipole Hamiltonian is not averaged identically to zero and a residual dipole coupling Hamiltonian given by [2.325] is obtained. When the coupling is weak, the Hamiltonian is truncated to [2.328]. This Hamiltonian and the weak scalar coupling Hamiltonian have the same functional form. Therefore, through-space coherence transfer under the residual dipole coupling Hamiltonian is obtained by COSY-type approaches identical to those described in Section 4.2.1.1 for through-bond coherence transfer under the scalar coupling Hamiltonian.

Circumstances are different if an isotropic mixing sequence is applied to a system of weakly aligned molecules. The mixing sequence, as for the analogous TOCSY experiment (Section 4.2.1.2), removes the chemical shift Hamiltonian, and evolution occurs under the full residual dipole coupling Hamiltonian given by [2.325]. However, in contrast to TOCSY transfer under the strong scalar coupling Hamiltonian, the residual dipole coupling Hamiltonian [2.325] is not isotropic. In the presence of the mixing sequence, the spin operators in [2.325] are averaged by rotation. For a mixing sequence applied along the x-axis,

$$\begin{aligned}
\overline{2I_xS_x} &= 2I_xS_x, \\
\overline{2I_yS_y} &= 2I_yS_y\,\overline{\cos^2\theta} + \left(2I_yS_z + 2I_zS_y\right)\overline{\cos\theta\,\sin\theta} + 2I_zS_z\,\overline{\sin^2\theta} \\
&= I_yS_y + I_zS_z, \\
\overline{2I_zS_z} &= 2I_zS_z\,\overline{\cos^2\theta} - \left(2I_yS_z + 2I_zS_y\right)\overline{\cos\theta\,\sin\theta} + 2I_yS_y\,\overline{\sin^2\theta} \\
&= I_yS_y + I_zS_z,
\end{aligned} \qquad [4.27]$$

in which θ is the time-dependent rotation angle and averaging over the entire mixing sequence is denoted by the overbars. The effective residual dipole–dipole coupling Hamiltonian during the mixing sequence is given by

$$\mathscr{H} = -\tfrac{1}{2}\pi D_{IS}(2I_xS_x - 2I_yS_y - 2I_zS_z). \qquad [4.28]$$

As [4.27] makes clear, the isotropic strong scalar coupling Hamiltonian is unchanged by averaging during the mixing sequence. Evolution under the Hamiltonian [4.28] can be analyzed using the same approach used in Section 4.2.1.2. The resulting expressions for evolution of I_x and I_z magnetization are (*24*)

$$I_x \xrightarrow{\mathscr{H}\tau_m} I_x \tfrac{1}{2}(1+\cos\pi D_{IS}\tau_m) + S_x \tfrac{1}{2}(1-\cos\pi D_{IS}\tau_m) + \left(2I_yS_z - 2I_zS_y\right)\tfrac{1}{2}\sin\pi D_{IS}\tau_m, \qquad [4.29]$$

$$\begin{aligned} I_z \xrightarrow{\mathscr{H}\tau_m} & I_z\left\{\tfrac{1}{2}\cos\tfrac{3}{2}\pi D_{IS}\tau_m + \tfrac{1}{2}\cos\tfrac{1}{2}\pi D_{IS}\tau_m\right\} \\ & + S_x\left\{\tfrac{1}{2}\cos\tfrac{3}{2}\pi D_{IS}\tau_m - \tfrac{1}{2}\cos\tfrac{1}{2}\pi D_{IS}\tau_m\right\} \\ & + \left(2I_yS_x + 2I_xS_y\right)\tfrac{1}{2}\sin\tfrac{3}{2}\pi D_{IS}\tau_m + \left(2I_yS_x - 2I_xS_y\right)\tfrac{1}{2}\sin\tfrac{1}{2}\pi D_{IS}\tau_m. \end{aligned} \qquad [4.30]$$

Because the Hamiltonian is not isotropic, different transfer functions are obtained for the orthogonal I_x and I_z operators. Evolution of an initial density operator proportional to I_x is formally identical to the transfer obtained in the TOCSY experiment. In contrast, if the initial state of the density operator is proportional to I_z, [4.30] indicates that the diagonal peaks (proportional to I_z) and cross-peaks (proportional to S_z) have opposite signs. This unique property of evolution under the residual dipole coupling Hamiltonian can be used to identify evolution due to three-spin interactions (*24*).

In summary, homonuclear coherence transfer under the residual dipole–dipole Hamiltonian for partially aligned molecules in the presence of a mixing sequence has been termed the DCOSY (dipolar correlation spectroscopy) experiment (*24*). The resulting Hamiltonian is not isotropic and the coherence transfer amplitudes obtained depend on the initial state of the density operator.

4.3 Coherence Selection, Phase Cycling, and Field Gradients

Modern NMR experiments consist of the application of multiple rf pulses to the system under investigation and detection of the resulting resonance signals. These multipulse NMR techniques are described by the pulse sequences used to generate the observed signal and by the evolution of the density operator through the pulse sequence. If an experiment consists of multiple pulses and delays, then more than

one coherence transfer pathway that leads to observable signals may exist for the spin system of interest. A spectrum derived from many different but simultaneously occurring coherence transfer pathways would be extremely complex and difficult to interpret. Phase cycling or field gradients are used to select a specific pathway and provide an interpretable spectrum. Phase cycling refers to the process of repeating a pulse sequence several times with a systematic variation of the relative phases of the pulses within the sequence. Coherence selection by means of phase cycling normally is implemented during the process of signal averaging. Field gradients are spatially inhomogeneous magnetic fields that are activated for specific periods within a pulse sequence. Coherence selection using pulsed field gradients is achieved during a single repetition of the pulse sequence.

In the following sections, the principles of coherence selection with phase cycles and pulsed field gradients are illustrated. The text follows closely the excellent approach presented by Keeler (*25*) and employs the coherence transfer pathway methods of Bodenhausen (*26*).

4.3.1 COHERENCE LEVEL DIAGRAMS

The concept of coherence developed in Section 2.6 is crucial to an understanding of phase cycling and field gradient techniques. The order of a coherence between two eigenstates of a spin system is defined as $p = \Delta m$, in which Δm is the difference between the magnetic quantum numbers of the two eigenstates. If an arbitrary operator is expressed in the shift operator basis (Section 2.7.2), then the coherence order is given by the number of raising operators minus the number of lowering operators comprising the representation. Thus, the absolute value of p must be less than or equal to $p_{\max}$, which is given by the number of spins involved in the coupling network. Longitudinal magnetization, although not strictly a coherence, has properties in common with zero-quantum coherence and is treated as such for phase cycling procedures.

At any particular point during a pulse sequence, various coherences may be present simultaneously. Normally, only one, or a small number, of the possible coherences are retained to generate a useful signal. At any time, the coherences present are classified according to their various orders (double, single, zero, etc.), and each coherence order is said to correspond to a different coherence level. For example, double-quantum coherence has a coherence level of ± 2, and longitudinal magnetization has a coherence level of zero. Formally, the density operator, σ, is

written as the expansion

$$\sigma = \sum_{p=-p_{\max}}^{p_{\max}} \sigma_p, \qquad [4.31]$$

in which σ_p is the component of the density operator associated with a particular coherence level, p. The sum in [4.31] contains $2p_{\max}+1$ terms and consequently does not represent an expansion of the density operator into a complete set of basis functions, because a complete set consists of 4^p elements. Each term in [4.31] would have to be further subdivided to generate a complete basis set. For example, longitudinal magnetization and zero-quantum coherence are part of the same component σ_0 in [4.31] but are represented by two different orthogonal basis operators. Each term σ_p is given in terms of single transition operators by

$$\sigma_p = \sum_{a,b} c_{ab}|a\rangle\langle b|, \qquad [4.32]$$

in which the sum extends over all combinations of eigenstates $|a\rangle$ and $\langle b|$ for which the magnetic quantum numbers satisfy the relationship $m_a - m_b = p$.

The effects of a pulse sequence (i.e., pulses and periods of free precession) on coherence order are encapsulated in two rules: first, rf pulses can cause the transfer of coherence from one level to another, and second, periods of free precession conserve the order of coherence. Indeed, an rf pulse potentially can transfer coherence to *all* coherence levels available to the spin system. The generation of different coherence orders during an NMR experiment is subject to the following three corollaries: (*i*) the coherence transfer pathway must start at coherence level $p=0$, as this corresponds to thermal equilibrium longitudinal magnetization, (*ii*) only coherence orders $p=\pm1$ are created by an rf pulse acting on the thermal equilibrium density operator, and (*iii*) if the complex signal is observed using quadrature detection then the coherence pathway must end at $p=-1$.

As has been stated several times, most coherences generated during a pulse sequence are suppressed, and only the coherences that will generate the desired NMR spectrum are retained. Coherence is transferred in a specific manner between other coherences by rf pulses during a pulse sequence. The trace of coherence level changes that result in the desired NMR spectrum is known as the *coherence transfer pathway*. The objective is to use an appropriately designed phase cycle or application of an appropriate set of field gradient pulses to detect only

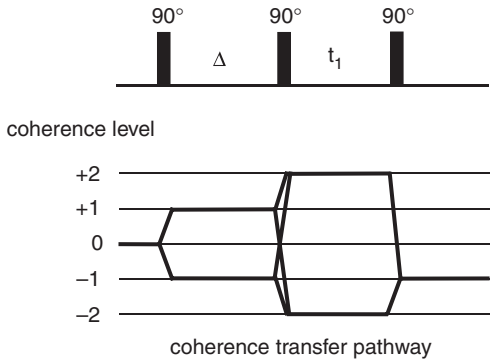

FIGURE 4.5 Coherence transfer pathway for a double-quantum experiment. Double-quantum coherence is selected during the t_1 period. The pathway indicated is only one of many pathways that are generated during the pulse sequence; unwanted coherence transfer pathways are rejected by phase cycling.

those signals that follow the chosen coherence transfer pathway. For example, in a two-dimensional double-quantum experiment (Section 6.4.1), the intention is to have double-quantum coherence evolve during t_1. The coherences present at each point in the pulse sequence are expressed conveniently using a coherence level diagram, as shown in Fig. 4.5 for a double-quantum experiment. The feasible coherence levels (-2, -1, 0, 1, 2 for a two-spin system) are shown as horizontal lines. The heavy solid lines trace the desired coherence transfer pathway by showing the desired coherence levels at every point in the pulse sequence. The indicated trace is only one of many possible coherence pathways that are generated by this particular pulse sequence. Pathways (not shown) that have coherence levels of -1, 0, or $+1$ during t_1 must be suppressed by the phase cycle or field gradient pulses.

4.3.2 PHASE CYCLES

Single-quantum coherence between two nuclear spin angular momentum states, or transverse magnetization, is responsible for the induction of a voltage in the receiver coil. Coherence is an oscillating function of time and is conveniently represented by a vector rotating in a circle (at least for an isolated spin treatable by the Bloch formalism). The angular position of this coherence "vector" at the beginning of the free induction decay determines the phase of the corresponding line in the spectrum. Conventionally, one axis (the reference axis) is chosen such that an absorption mode line is produced when the coherence

vector is aligned with this axis at the start of the acquisition period; other orientations of the vector give different phases of the resonance signal. Figure 4.6 illustrates the relationship between the phase of the rf pulse, the initial orientation of the coherence vector, and the phase of the resonance signal. An alternative way to change the phase of a resonance line is to shift the reference axis while keeping the pulse phase fixed.

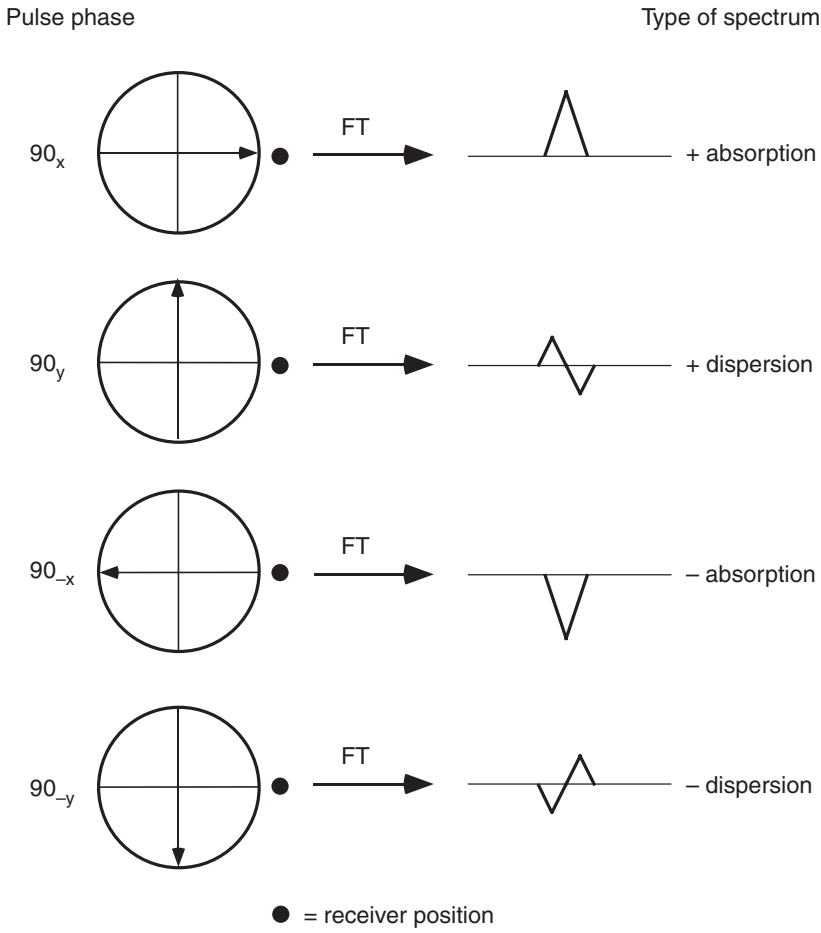

FIGURE 4.6 Pulse phase. The phase of a 90° pulse is shifted in increments of 90° while keeping the phase of the receiver constant. The phase of the resulting signal in a one-pulse experiment changes in conjunction with the phase change of the pulse. Co-addition of the four resonance signals results in the cancellation of the signal.

Figure 4.7 illustratesthe relationship between the receiver phase and the phase of the resonance signal. Comparison of Figs. 4.6 and 4.7 indicates that a given phase difference in the signal is achieved equally well by adjusting the phase of the rf pulses or of the receiver.

Referring to the block diagram of an NMR spectrometer shown in Chapter 3 (Fig. 3.1), the receiver phase can be adjusted in two ways: the phase of the rf reference signal in the phase-sensitive detector can be

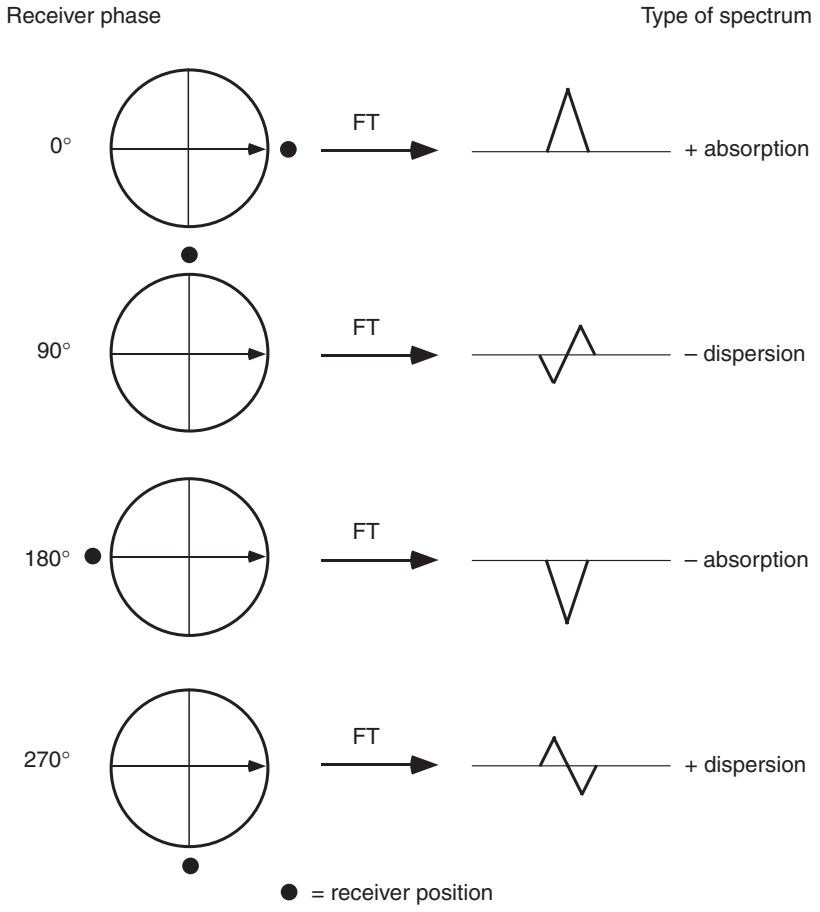

FIGURE 4.7 Receiver phase. The phase of the receiver is shifted in increments of 90° while keeping the phase of the 90° pulse constant. The phase of the resulting signal in a one-pulse experiment changes in conjunction with the phase change of the receiver. Co-addition of the four resonance signals results in the cancellation of the signal.

changed (see also Fig. 3.5) and the digitizer phase can be changed. A change in digitizer phase really is a purely digital manipulation of the FID in computer memory. A 180° digitizer phase shift is obtained by negating the data after they have been digitized in the ADC; a 90° digitizer phase shift is obtained by exchanging the real and imaginary parts of the complex signal after they have been digitized in the ADC. Herein, a distinction between these two approaches to shifting the receiver phase rarely needs to be made; however, the effects of imperfections in components in the phase-sensitive detector, such as electrical dc (nonsinusoidal) baseline offset and gain imbalance in the receiver channels (Section 4.3.2.3), only can be eliminated by phase cycling executed on the digitizer phase.

If the pulse is cycled through the four phases, x, y, $-x$, and $-y$, on four successive experiments and the transients added together (in either the time or frequency domain), then a null signal is obtained because the two absorptive signals are exactly 180° out of phase with each other, as are the two dispersive signals. A similar result is obtained for the transients shown in Fig. 4.7. However, if the phase of the pulse is cycled and the receiver phase is moved in concert to track the change in the phase of the coherence, then each transient results in an absorption signal with the same phase, as shown in Fig. 4.8. If the four experiments are combined, the signals add constructively and a final spectrum is obtained that contains a single absorption line.

This simple example, which forms the basis of the CYCLOPS technique (Section 4.3.2.3), illustrates the basic principle of phase cycling. The signal of interest is forced to change phase, by shifting the phase of rf pulses, in conjunction with the receiver, so as to cause the signal recorded from different transients to accumulate. In the same manner, unwanted signals are suppressed by ensuring that signals recorded from a series of transients cancel.

4.3.2.1 Selection of a Coherence Transfer Pathway The property used to select a specific coherence transfer pathway by phase cycling is as follows:

> *If a pulse is changed in phase by an amount, ϕ, then a coherence undergoing a change in coherence level of Δp, due to that pulse, acquires a phase shift of $-\Delta p\phi$.*

For example, consider a coherence at level +3 being transferred to level +1 by the action of a pulse. If, during the experiment the pulse changes phase by ϕ, then the coherence will acquire phase $-\Delta p\phi$, where

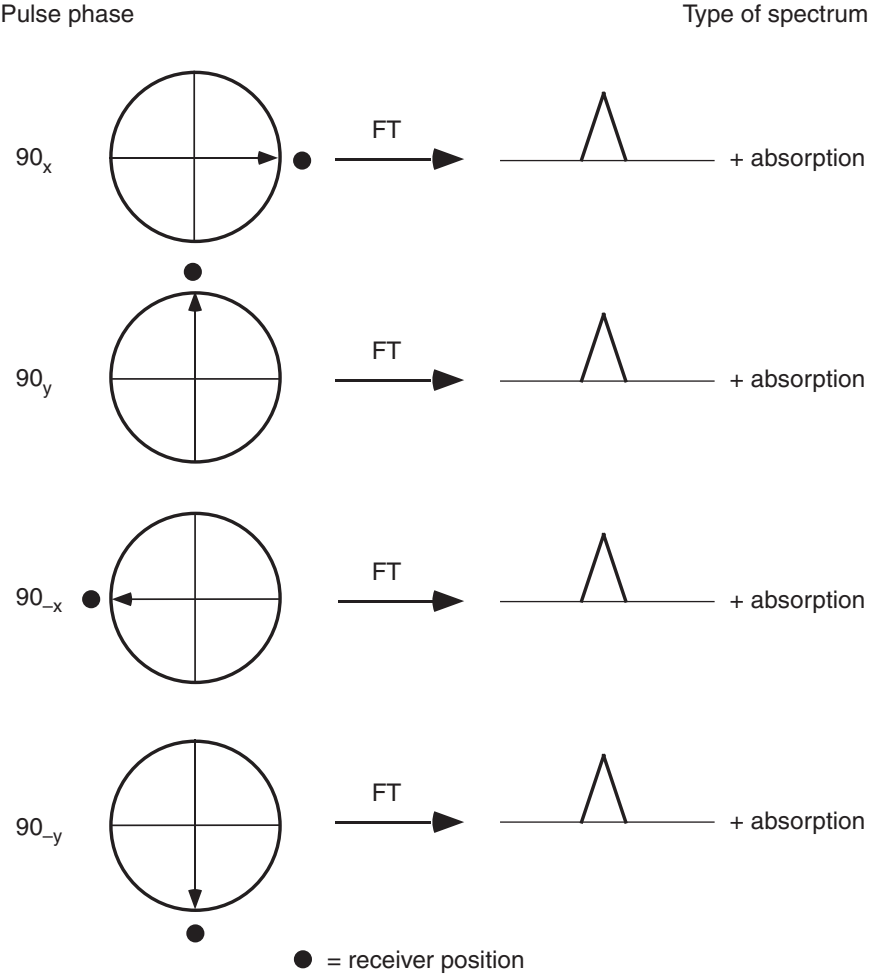

FIGURE 4.8 Pulse and receiver phase. The phase of the 90° pulse is shifted in increments of 90° while simultaneously shifting the phase of the receiver in increments of 90°. In this case, the resulting signal retains the same phase in each experiment (shown as absorptive here). Co-addition of the four resonance signals results in the coherent summation of the signal.

$\Delta p = (+1) - (+3) = -2$. Thus the coherence acquires phase $+2\phi$. The coherences are labeled with phase shifts during the pulse sequence. The ultimate phase of the observed magnetization depends on the total phase angle that the coherence acquires during the coherence transfer steps in the sequence. The accumulated phase angles of the desired

coherence transfer pathway enable its selection. Coherence selection is accomplished simply by changing the phases of the relevant pulses in the sequence by the appropriate amounts.

To prove the preceding statement, the effect on a particular coherence of a nonselective z-rotation (affecting all spins identically) is proved first:

$$\begin{aligned}\exp(-i\phi\mathbf{F}_z)\sigma_p \exp(i\phi\mathbf{F}_z) &= \sum_{a,b} c_{ab} \exp(-i\phi\mathbf{F}_z)|a\rangle\langle b| \exp(i\phi\mathbf{F}_z) \\ &= \sum_{a,b} c_{ab} \exp(-i\phi m_a)|a\rangle\langle b| \exp(i\phi m_b) \\ &= \sum_{a,b} c_{ab}|a\rangle\langle b| \exp(-i\phi p) \\ &= \sigma_p \exp(-i\phi p). \end{aligned} \quad [4.33]$$

Next suppose that some propagator $\mathbf{U}$ transfers coherence from an element σ_p to an element σ_q:

$$\sigma_q = \mathbf{U}\sigma_p\mathbf{U}^{-1}. \quad [4.34]$$

If all rf pulses are shifted in phase by an angle ϕ, then (note that the Zeeman and scalar coupling interactions are unaffected by z-rotations)

$$\begin{aligned}&\exp(-i\phi\mathbf{F}_z)\mathbf{U} \exp(i\phi\mathbf{F}_z)\sigma_p \exp(-i\phi\mathbf{F}_z)\mathbf{U}^{-1} \exp(i\phi\mathbf{F}_z) \\ &\quad = \exp(-i\phi\mathbf{F}_z)\mathbf{U}\sigma_p \exp(i\phi p)\mathbf{U}^{-1} \exp(i\phi\mathbf{F}_z) \\ &\quad = \exp(-i\phi\mathbf{F}_z)\sigma_q \exp(i\phi\mathbf{F}_z) \exp(i\phi p) \\ &\quad = \sigma_q \exp(-i\phi q) \exp(i\phi p) \\ &\quad = \sigma_q \exp(-i\phi\Delta p), \end{aligned} \quad [4.35]$$

with $\Delta p = q - p$, which provides the desired proof.

Phase shifts of the receiver are represented by applying z-rotations to the detection operator $\mathbf{F}^+$:

$$\exp(-i\phi_{\text{rec}}\mathbf{F}_z)\mathbf{F}^+ \exp(i\phi_{\text{rec}}\mathbf{F}_z) = \mathbf{F}^+ \exp(-i\phi_{\text{rec}}). \quad [4.36]$$

Clearly, to coherently accumulate signals from a desired coherence transfer pathway,

$$\text{Tr}\{\sigma(t)\mathbf{F}^+\} = \text{Tr}\{\sigma(t)\mathbf{F}^+\} \exp(-i\phi\Delta p) \exp(-i\phi_{\text{rec}}), \quad [4.37]$$

and $\phi_{\text{rec}} = -\phi\Delta p$. Thus, as already noted, the receiver phase shifts must follow the phase shifts accrued by the density operator through the series of pulse phase cycles.

To illustrate the use of phase cycling to retain one coherence transfer pathway while rejecting another, suppose that in some pulse sequence a mixture of double-quantum coherence ($p = \pm 2$) and zero-quantum coherence ($p = 0$) has been created. Application of a 90° pulse to the initial zero- and double-quantum states causes the desired and undesired transfers between coherence levels shown in Fig. 4.9. The goal of the phase cycle is to convert double-quantum coherence to observable single-quantum coherence ($p = -1$) while suppressing any signal from the zero-quantum coherence.

The experiment is repeated four times; upon each repetition, the phase of the pulse is incremented by 90° to yield a phase cycle of 0°, 90°, 180°, 270° (which conventionally is written as x, y, $-x$, $-y$). The desired

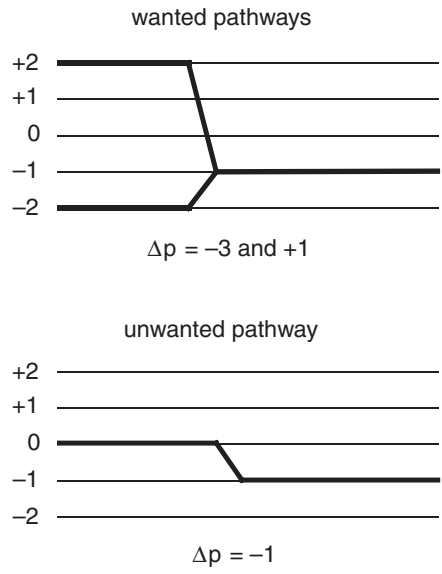

FIGURE 4.9 Selection of double-quantum coherence. The upper part of the figure illustrates the desired coherence transfer pathways corresponding to coherence-level changes from double-quantum ($p = +2$ and -2) to observable single-quantum ($p = -1$) coherence. These pathways have coherence order changes of $\Delta p = -3$ and $+1$, respectively. The lower part of the figure illustrates the coherence transfer pathway to be rejected corresponding to a coherence-level change from zero-quantum ($p = 0$) to observable single-quantum ($p = -1$) coherence. This pathway has a coherence order change of $\Delta p = -1$.

coherence ($p = \pm 2$) goes through two pathways, with $\Delta p = -3$ ($p = +2$ to $p = -1$) and $\Delta p = +1$ ($p = -2$ to $p = -1$). The coherence that undergoes the level change $\Delta p = -3$ changes phase by an amount $-\Delta p\phi = -(-3)\phi = +3\phi$. The acquired phase of the observable coherence for the four transients will be 0°, 270°, 540°, 810°, or in terms of 0° to 360° rotations, 0°, 270°, 180°, 90°. In a similar way, the coherence undergoing a level change of $\Delta p = +1$ acquires a phase of $-\Delta p\phi = (-1\phi) = -\phi$. The coherence acquires phase 0°, –90°, –180°, –270°, which in the 0° to 360° reference frame is equivalent to 0°, 270°, 180°, 90°. Thus, in the experiment described, the two coherence level changes of $\Delta p = -3$ and $\Delta p = +1$ result in the observable coherences acquiring phase in an identical fashion. To ensure that the required signal (from both pathways) accumulates constructively on successive transients, then the receiver phase must follow exactly the phase shifts of the wanted coherence. Therefore the receiver phase cycle is 0°, 270°, 180°, 90°. This information is contained in Table 4.1.

The coherence level change from zero-quantum coherence to observable single-quantum coherence has $\Delta p = -1$. Employing the same analysis as previously, the coherence acquires phase $-\Delta p\phi = -(-1\phi) = +\phi$, or 0°, 90°, 180°, 270°. This result, along with the receiver phase cycle determined previously, is tabulated in Table 4.2. While steps 1 and 3 of the receiver phase cycle follow the coherence, steps 2 and 4 are exactly opposite to the coherence phase. Consequently, the same phase cycle, including pulse and receiver phase shifts, that retains the wanted

TABLE 4.1
Selection of Double-Quantum Coherence

Pulse phase (ϕ)	$-\Delta p\phi$	Equivalent cycle	Receiver phase
	Coherence change $\Delta p = -3$		
0	0	0	0
90	270	270	270
180	540	180	180
270	810	90	90
	Coherence change $\Delta p = +1$		
0	0	0	0
90	−90	270	270
180	−180	180	180
270	−270	90	90

TABLE 4.2
Rejection of Zero-Quantum Coherence

Pulse phase (ϕ)	$-\Delta p\phi$	Equivalent cycle	Receiver phase
	Coherence change $\Delta p = -1$		
0	0	0	0
90	90	90	270
180	180	180	180
270	270	270	90

pathways ($\Delta p = -3$ and $\Delta p = +1$) also serves to eliminate the unwanted pathway ($\Delta p = -1$), exactly as required.

In the preceding example, a four-step phase cycle with increments in phase of 90° was able to discriminate between coherence transfer pathways of $\Delta p = -3$, $+1$ and $\Delta p = -1$. The effect of this phase cycle is represented conveniently using the nomenclature of Bodenhausen and co-workers, as: $-\mathbf{3}$ (-2) (-1) (0) $\mathbf{+1}$ $(+2)$ $(+3)$, where the pathways passed by the cycle are set in bold and the pathways blocked by the cycle are set in parentheses. Under the proposed scheme, *two* pathways are allowed to pass. In general, if a phase cycle uses increments in phase of $360/N$ degrees, then along with the pathway Δp selected, pathways $\Delta m = \Delta p \pm nN$, where $n = 1, 2, 3\ldots$, will also be selected. Bodenhausen showed that the length and selectivity of a phase cycle are related (26). If a particular value of Δp is to be chosen from r consecutive values, then N must be at least r. In practical terms, increased selectivity in choosing a specific coherence transfer pathway requires a larger number of smaller steps in the phase cycle.

Continuing with the preceding example, now consider discriminating between the two pathways $\Delta p = -3$ and $\Delta p = +1$, both of which were retained by the original phase cycle. For instance, suppose only the $\Delta p = +1$ pathway is to be retained and the $\Delta p = -3$ pathway is to be rejected. Table 4.3 shows the effects of extending the phase cycle to six steps rather than four and using a phase increment of 60° rather than 90°. The analysis proceeds exactly as before, making sure that the receiver shifts in phase so as to follow the phase acquired by the coherence going through the $\Delta p = +1$ pathway.

Consulting Table 4.3, the signal from the $\Delta p = +1$ pathway will add on all transients. However, the effect of this receiver phase cycle on the signal arising from the $\Delta p = -3$ pathway is not obvious. In the approach adopted by Keeler (*25*), the net effect of the phase cycle is represented by

TABLE 4.3
Distinguishing $\Delta p = +1$ from $\Delta p = -3$

Pulse phase (ϕ)	$-\Delta p\phi$	Equivalent cycle	Receiver phase
	Coherence change $\Delta p = +1$		
0	0	0	0
60	−60	300	300
120	−120	240	240
180	−180	180	180
240	−240	120	120
300	−300	60	60
	Coherence change $\Delta p = -3$		
0	0	0	0
60	180	180	300
120	360	0	240
180	540	180	180
240	720	0	120
300	900	180	60

subtracting the phase acquired by the coherence from the receiver phase (or *vice versa*) and representing the differences as a vector diagram. The Equivalent cycle and Receiver phase in Table 4.3 are reproduced in columns A and B of Table 4.4. Subtracting column A from column B gives the results shown in Table 4.4. Figure 4.10 shows that the net effect of the vectors is zero, indicating any signal resulting from the $\Delta p = -3$ pathway will be canceled.

As anticipated, a longer phase cycle with smaller phase increments on each step allows greater selectivity. Remembering the rules noted

TABLE 4.4
Rejecting $\Delta p = -3$

Coherence phase [A]	Receiver phase [B]	[B] – [A]	Equivalent phase [B] – [A]
0	0	0	0
180	300	120	120
0	240	240	240
180	180	0	0
0	120	120	120
180	60	–120	240

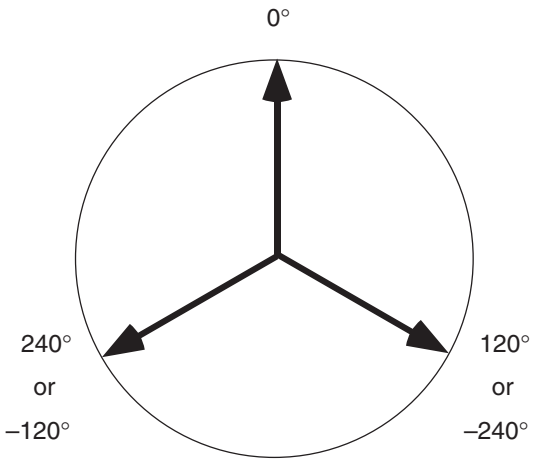

FIGURE 4.10 Vectorial picture of phase cycling. From the results in Table 4.4, vectors are drawn corresponding to the difference in phase acquired by the coherence and the receiver phase, for the coherence transfer pathway $p = +2$ to $p = -1$ ($\Delta p = -3$). In this case, the goal is to discriminate between the coherence order change $\Delta p = +1$ and $\Delta p = -3$. The sum of these vectors is zero, and any signal from the $\Delta p = -3$ pathway is eliminated.

earlier, this phase cycle will also retain pathways where $\Delta p = +1 \pm 6n$. All other pathways are rejected. Using the nomenclature of Bodenhausen (*26*), the effect of this phase cycle is written as (−6) **−5** (−4) (−3) (−2) (−1) (0) **+1** (+2) (+3) (+4) (+5) (+6) **+7**. In fact, the six-step phase cycle used in this example is overly selective; as the notation of Bodenhausen makes clear, a five-step phase cycle with 72° increments would also have been satisfactory (although more difficult to visualize).

The preceding principles can be restated as follows:

1. A phase cycle (affecting a single rf pulse or a group of pulses) that consists of N steps with $\Delta\phi = 360°/N$ increments selects coherence transfer pathways satisfying $\Delta m = \Delta p \pm nN$, in which n is an integer.
2. The value of Δp is selected, from the N consecutive possible values Δp, $\Delta p + 1$, $\Delta p + 2, \ldots, \Delta p + N - 1$, by shifting the receiver phase by $\Delta\phi_{\text{rec}} = -360° \Delta p/N$ synchronously with the pulse phase cycle.

4.3.2.2 Saving Time To unambiguously select a definite coherence transfer pathway in a pulse sequence, each pulse must have a specific phase cycle and each phase cycle must be executed independently. Unfortunately, strict application of this rule generates extremely long

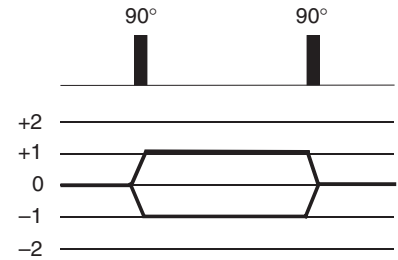

FIGURE 4.11 Two-pulse segment used to generate zero-quantum coherence.

phase cycles, and some mechanisms must be found to reduce the phase cycle to an acceptable length.

Rather than considering a coherence transfer step as being mediated by just one pulse, several pulses and intervening delays can be grouped together and regarded as a single unit that causes the desired coherence transfer. The phases of all the pulses in the unit are shifted simultaneously in order to reduce the number of steps in the overall phase cycle. For example, consider the two-pulse experiment shown in Fig. 4.11. The overall aim is to select the overall pathway $\Delta p = 0$ (coherence that starts at level 0 and ends at 0). Cycling each of the pulses independently in 90° increments to select the coherence transfer pathway shown results in a phase cycle of 16 steps. Phase cycling both the pulses simultaneously through the four phases 0°, 90°, 180°, 270°, while holding the receiver phase constant, selects the pathway $\Delta p = 0$ as required (this assertion can be checked by using the identity previously described, $\phi_{rec} = -\Delta p\phi$). In this way the phase cycle has been reduced from 16 steps to 4 steps. Note that all other pathways that have $\Delta p = 0$ will also be retained, because this approach leaves the coherence level between the pulses undefined. In many circumstances, these other pathways may be disregarded when additional considerations (discussed later) are taken into account. However, if an undesired coherence with $\Delta p = 0$ results in observable signals when the 4-step phase cycle is used, then the full 16-step phase cycle must be employed.

Normally the first pulse in a sequence is applied to equilibrium magnetization and only coherences with $\Delta p = \pm 1$ are generated. Indeed, a phase cycling scheme will only work if the same initial state exists for successive transients, and consequently suitable delays must be inserted between each transient to enable the system to return to equilibrium. Unless a specific reason exists for distinguishing the coherence levels +1

and –1 following the first pulse, then phase cycling of that pulse formally is unnecessary. However, the present theoretical discussion ignores relaxation and other effects that may make phase cycling of the first pulse desirable in practice (Section 4.3.2.3). If an unambiguous coherence transfer pathway has been chosen by the phase cycles of earlier pulses in the sequence, then the last pulse does not need to be phase cycled. Although application of the last pulse to the system may generate many different coherence orders and therefore many coherence pathways, only those pathways that lead to a final coherence level of $p = -1$ (single-quantum coherence) are observable. The experiment, in essence, chooses the last coherence transfer step itself.

Certain coherence transfer pathways are improbable in a given spin system. The maximum coherence available in a system is restricted by the number of nuclear spins in that system. For spin-1/2 nuclei, at least N coupled spins are required to produce N-quantum coherence. In principle, phase cycles that discriminate against coherence orders higher than N are unnecessary. In practice, generating large magnitudes of high-order coherences is difficult, even if theoretically possible, and coherence transfer pathways containing these coherence levels can be ignored. For example, coherence orders greater than four or five in ^{1}H spin systems may not require consideration and the resulting phase cycles can be correspondingly shorter. An alternative approach to designing phase cycling procedures, called *cogwheel phase cycling*, offers shorter phase cycles in some applications (*27, 28*).

4.3.2.3 Artifact Suppression Before continuing, three simple phase cycling procedures that are employed to reduce instrumental artifacts are discussed: CYCLOPS, EXORCYCLE, and axial peak suppression.

Quadrature detection is obtained during acquisition of the NMR signal by two phase-sensitive detection channels (Section 3.2.2). The two channels, in principle, should be identical except for a relative phase shift of 90°. Anomalies arise if differences exist between the two phase-sensitive detector channels. If the two quadrature channels have different sensitivities or are not completely orthogonal, then the NMR spectrum contains spurious peaks called *quadrature images*. The images are located in symmetric positions with respect to the center of the spectrum as genuine peaks (i.e., if a resonance has an offset of Ω, then the quadrature image appears at $-\Omega$). Also, if the electrical dc (nonsinusoidal) baseline offset between the two channels differs, then a spike appears in the middle of the spectrum. This artifact most commonly is referred to as a *quadrature glitch*.

In order to remove these artifacts, a simple phase cycling routine known as CYCLOPS is used (*29*). For the case of a simple pulse–acquire experiment, CYCLOPS consists of cycling the pulse and receiver through the phases 0°, 90°, 180°, 270° synchronously. Any gain difference between the two channels is compensated for by the 90° phase incrementation, while baseline offset errors are eliminated by the 180° phase inversions. As discussed in Section 4.3.2.2, dc baseline offset differences between receiver channels only can be suppressed if the digitizer phase is inverted. For longer and more complicated pulse sequences, a phase cycle normally is employed that closely mimics the action of CYCLOPS. If this is not the case, CYCLOPS is implemented by adding the phase incrementations 0°, 90°, 180°, 270° to *all* pulses in the sequence along with the receiver. The one drawback to this procedure is that the length of the phase cycle, and therefore the minimal experimental time, is increased by a factor of four. If phase cycling limitations preclude full CYCLOPS phase cycling in a particular pulse sequence, a two-step phase cycle consisting of 0° and 90° phase shifts may be satisfactory in reducing quadrature image artifacts (but not quadrature glitches). As an alternative to CYCLOPS, spectra that are free of quadrature artifacts can be obtained using digital filter technology implemented on modern NMR spectrometers (Section 3.2.3).

To illustrate the CYCLOPS technique more fully, an imbalanced detection operator is defined as

$$\mathbf{F}^+(\varepsilon) = I_x + i(1+\varepsilon)I_y = I^+ + \varepsilon/2(I^+ - I^-) = (1+\varepsilon/2)I^+ - \varepsilon/2I^-, \tag{4.38}$$

in which $\varepsilon \neq 0$ is the imbalance term. The detected signal is given as usual by the trace of the density operator with the detection operator:

$$\begin{aligned} s^+(t) &= \mathrm{Tr}\{\sigma(t)\mathbf{F}^+(\varepsilon)\} = \sum_{-p_{\max}}^{p_{\max}} \mathrm{Tr}\{\sigma_p(t)\mathbf{F}^+(\varepsilon)\}, \\ &= (1+\varepsilon/2)\,\mathrm{Tr}\{\sigma_{-1}(t)I^+\} - (\varepsilon/2)\,\mathrm{Tr}\{\sigma_{+1}(t)I^-\}. \end{aligned} \tag{4.39}$$

If $\varepsilon \neq 0$, any components of the density operator that are proportional to I^+, which has $p = +1$, will have a nonzero trace with the I^- operator and generate artifacts in the NMR spectra. Referring back to the concepts of coherence transfer pathways, CYCLOPS phase cycling is equivalent to selecting $\Delta p = -1$ for the entire sequence. Thus, assuming that the initial density operator is given by the thermal equilibrium operator,

$$s^+(t) = \mathrm{Tr}\{\sigma_{-1}(t)\mathbf{F}^+\} = (1+\varepsilon/2)\,\mathrm{Tr}\{\sigma_{-1}(t)I^+\}, \tag{4.40}$$

and the artifacts in the spectrum are suppressed.

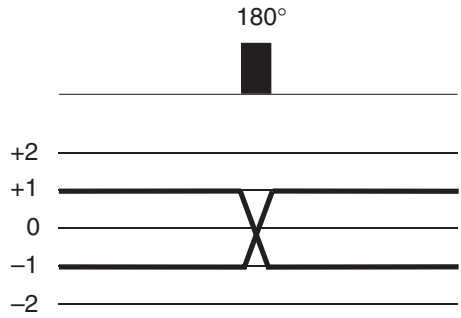

FIGURE 4.12 EXORCYCLE. Coherence transfer pathway for a spin echo sequence. The 180° pulse serves to change the sign of the coherence order.

The spin echo sequence, τ–180°–τ, is a vital component of a large number of NMR experiments. The coherence level diagram for this pulse sequence is shown in Fig. 4.12. Spin echo sequences are sensitive to common imperfections in 180° pulses, such as miscalibrated pulse lengths and off-resonance effects, that can generate spurious responses. The EXORCYCLE phase cycling scheme is designed to compensate for imperfect 180° pulses (*30*). An ideal 180° refocusing pulse simply has the effect of changing the sign of the coherence level. For example, if the initial density operator has coherence level $p = +1$, then following the 180° pulse the coherence level would be $p = -1$. The desired coherence transfer pathway has $\Delta p = -2$, so the appropriate phase cycle for the 180° pulse would be 0°, 90°, 180°, 270°, while the receiver is cycled 0°, 180°, 0°, 180°. This is the EXORCYCLE phase cycle. This phase cycle also selects the mirror image pathway $\Delta p = +2$ so that the EXORCYCLE procedure can be employed if the spin echo segment is part of a more complicated sequence (Section 4.3.4). The undesired pathway of $\Delta p = 0$, which corresponds to unrefocused magnetization, and $\Delta p = \pm 1$, which corresponds to a coherence transfer process, are both suppressed by the EXORCYCLE procedure. If suppression of $\Delta p = 0$ is not important in a particular application, then a two-step phase cycle can be utilized, in which the 180° pulse is cycled by 0° and 180° and the receiver phase is not altered.

Axial peaks occur in multidimensional NMR experiments because magnetization relaxes toward equilibrium during free-precession evolution periods, such as the t_1 interval. This magnetization is not frequency labeled during the t_1 period, and is not sensitive to the phase cycling of

pulses occurring earlier in the sequence. If the relaxed longitudinal magnetization is converted to observable magnetization prior to the acquisition period, then spurious signals will be generated along the line $F_1 = 0$ in the NMR spectrum (see Section 4.3.4.3). Axial peaks are eliminated by phase cycling a pulse or pulses prior to the t_1 period and the receiver by phase angles of 0° and 180°. The most common procedure for obtaining axial peak suppression is by phase cycling the initial pulse in the pulse sequence in conjunction with the receiver. This phase cycle selects $\Delta p = \pm 1$, corresponding to creation of transverse magnetization by the first pulse. Many multidimensional NMR experiments have complex phase cycles that function incidentally to suppress axial peaks.

4.3.2.4 Limitations of Phase Cycling A phase cycle works by requiring signals arising from the desired coherence transfer pathway to add constructively on successive transients, whereas signals from unwanted pathways cancel. Evidently, phase cycling is simply a difference method and consequently will only work if experimental conditions remain constant from transient to transient. Unfortunately, as a practical matter, slight variations occur between transients. For example, amplitude or phase changes in the pulses or field frequency variations in the lock circuitry can contribute to variability from transient to transient and reduce the effectiveness of phase cycling. One of the most common sources of instability is temperature fluctuations that cause resonances (including the lock resonance) to shift slightly.

The magnitude of the signals derived from the desired coherence transfer pathway compared to the magnitude of signals from unwanted pathways is an important determinant in the success of phase cycling. If signals from unwanted pathways are expected to be large, errors in the difference procedure may produce artifacts of intensity comparable to the intensity of desired signals. Although the deleterious effects of random fluctuations on coherence selection would be expected to cancel after extended signal averaging, instrumental instabilities are frequently periodic, and even for random effects convergence is generally slow. From a practical point of view, the order in which the individual steps of the phase cycle are employed may result in better or worse suppression of undesirable signals. Unfortunately, the particular order that the steps in a phase cycle should be applied can vary from one spectrometer to another and must be determined empirically.

Phase cycles also assume that at the beginning of each transient the system is in thermal equilibrium and only longitudinal magnetization exists. Leaving a long recycle time between successive transients is the optimum way to ensure this condition, but this approach can cause

lengthy experiments, and recycle times on the order of $1/R_1$ to $1.5/R_1$ are commonly employed. In some instances, the phase cycle is designed to suppress artifacts that arise from rapid repetition of a pulse sequence.

4.3.3 PULSED FIELD GRADIENTS

An alternative method for coherence transfer pathway selection has been developed that makes use of pulsed field gradients and avoids many of the problems associated with phase cycling procedures (*31–41*). Dephasing of transverse magnetization by a field gradient pulse is described by [3.131] in Section 3.5.3. For application in coherence selection, this result is generalized to include coherences of arbitrary order. The critical principle, easily obtained by an approach similar to that employed in deriving [3.131], is based on [3.132] and is stated as follows:

> *Coherence dephases in an inhomogeneous magnetic field at a rate proportional to the coherence order and the magnetogyric ratios of the affected nuclei.*

4.3.3.1 Selection of a Coherence Transfer Pathway A particular coherence transfer pathway is selected by using field gradient pulses to generate gradient echoes for specific coherences, while leaving unwanted coherences randomized. Consider the case in which field gradient pulses are applied on either side of a mixing period that mediates coherence transfer between coherence levels p_i and p_f. The first gradient pulse, applied with a shape factor s_1, a strength B_{g1}, and a duration t_1, induces a spatially dependent phase of ϕ_i, and the second gradient pulse, applied with a shape factor s_2, a strength B_{g2}, and a duration t_2, induces a phase of ϕ_f, where

$$\begin{aligned} \phi_i &= s_1 p_i \gamma_i B_{g1} t_1, \\ \phi_f &= s_2 p_f \gamma_f B_{g2} t_2, \end{aligned} \qquad [4.41]$$

in which γ_i and γ_f are the magnetogyric ratios of the nuclei comprising the two coherences. Following the second gradient pulse, the net phase accrued by the final coherence is $\phi_i + \phi_f$. Selection of a *particular* coherence transfer pathway $p_1 \rightarrow p_2$ occurs by ensuring that the overall phase change is zero; therefore, the durations and amplitudes of the two gradient pulses must be adjusted such that $\phi_1 = -\phi_2$. The second gradient can be thought to "unwind" the effects of the first gradient

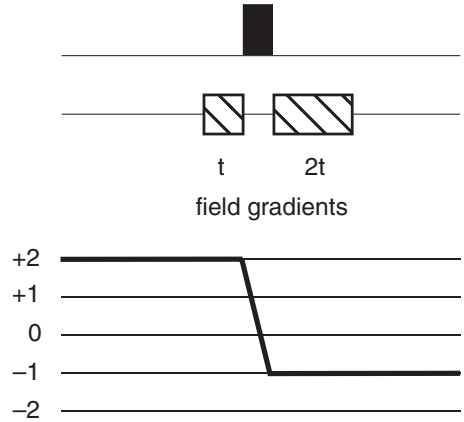

FIGURE 4.13 Selection of the coherence transfer pathway $p=+2$ to $p=-1$ by the use of pulsed field gradients. The double-quantum coherence $p=+2$ accrues a phase proportional to $+2t$, in which t is the duration of the first gradient pulse. The following rf pulse (solid bar) transfers the coherence to $p=-1$. To rephase *only* the final coherence that originated at the $p=+2$ coherence level, application of the second gradient, for duration $2t$, serves to "unwind" exactly the required coherence.

to form an echo. Coherence orders for which $\phi_i+\phi_f\neq 0$ remain dephased and do not contribute to the resulting signal.

An illustrative example of coherence selection by gradient pulses is shown in Fig. 4.13. In this example a gradient is applied for a time t prior to the pulse that causes the coherence transfer. The coherence $p=+2$ dephases by an amount that is proportional to $+2t$. The pulse transfers the coherence to $p=-1$, then a gradient, in the same sense, is reapplied, but this time for a time $2t$. The coherence at this level dephases by an amount proportional to $-2t$, which is in an opposite sense to that induced by the first gradient pulse. Consequently, after a time $2t$, the required coherence is fully rephased. By using strong field gradients, all other coherences involved in other pathways are dephased and coherence selection is achieved.

The real advantage of gradient pulses, compared with phase cycling, is that signals arising from unwanted pathways are removed by the gradients in each individual transient rather than relying on subtraction processes after digitization of the signal. Consequently, artifacts from instrumental instabilities may be significantly smaller than in

experiments using phase cycling for coherence selection. In addition, for some experiments, the number of transients that must be accumulated to achieve a particular signal-to-noise ratio is smaller than the number of transients required to select a particular coherence transfer pathway by phase cycling procedures; the experiment can be executed in less time if gradient pulses are used for coherence selection. This attribute becomes important when recording higher dimensional experiments that require large amounts of spectrometer time.

4.3.3.2 Artifact Suppression Artifact suppression using CYCLOPS and EXORCYCLE phase cycling was discussed in Section 4.3.2.3. Implementation of these schemes requires a minimum number of phase cycle steps, and employing more than one of these schemes can increase the length of a phase cycle enormously (i.e., independent EXORCYCLE phase cycling of n 180° pulses requires 4^n steps). To reduce such prolonged phase cycles, very simple combinations of gradients are used for artifact suppression. In practice, three- and four-dimensional experiments, with correspondingly large numbers of pulses, coherence transfer steps, and refocusing periods, exhibit the most artifacts and are subject to the most severe restrictions on the overall length of the phase cycle. The performance of a number of common components of heteronuclear multidimensional NMR experiments is augmented by the introduction of appropriate pulsed field gradients (*42*).

The 180° refocusing pulse in a spin echo sequence is notoriously prone to pulse artifacts that historically would be removed by the EXORCYCLE phase cycle. The gradient-enhanced homonuclear spin echo sequence is

$$\begin{array}{ccccc} \tau & & -180^\circ(I)- & & \tau \\ +z\text{-gradient} & & & & +z\text{-gradient.} \end{array} \qquad [4.42]$$

A transverse operator — for example, either I_x or I_y — is dephased by the first gradient, the coherence order is inverted by the 180°(I) pulse, and then the operator is rephased by a gradient *of the same sign and the same strength*. The gradient pulses eliminate the effect of pulse imperfections that lead to transfer between transverse and longitudinal magnetization and, additionally, any transverse operator of a different spin not affected by the 180° pulse is effectively removed. This is all accomplished *in a single transient*.

In another common application, a 180°(I) heteronuclear decoupling pulse is used to invert the longitudinal I spin component of antiphase

heteronuclear coherence, $2I_zS_x$ or $2I_zS_y$, from $+z$ to $-z$ (or *vice versa*). This serves to decouple the two spins during the time period 2τ:

$$\begin{array}{ccc} \tau & -180^\circ(I)- & \tau \\ +z\text{-gradient} & & -z\text{-gradient.} \end{array} \qquad [4.43]$$

The z-component inverted by the 180° pulse is unaffected by the application of either gradient. The $+z$ and $-z$ gradients refocus the transverse S magnetization. Conversion of z-magnetization into transverse magnetization by an imperfect $180^\circ(I)$ pulse is eliminated because such transverse magnetization will be irreversibly dephased by the second gradient. Again, artifact suppression is accomplished in one transient.

In INEPT (Section 2.7.7.2) and other coherence transfer sequences, evolution under the scalar coupling Hamiltonian converts in-phase magnetization into antiphase coherence — for example, $I_y \rightarrow I_y \cos(\pi J_{IS}t) - 2I_xS_z \sin(\pi J_{IS}t)$. Longitudinal two-spin order, $2I_zS_z$, is created from the antiphase coherence, $2I_xS_z$, by application of a $90^\circ(I)$ pulse with y-phase. Two-spin order has a coherence order of zero and is unperturbed by gradient pulses. Accordingly, the residual I_y magnetization, resulting if $t \neq 1/(2J_{IS})$, for example, is selectively dephased by applying a field gradient pulse after the creation of two-spin order. However, other operators with coherence order zero, such as longitudinal magnetization, also are unperturbed by gradient pulses. In the case of zero-quantum (ZQ) coherence, the efficacy of dephasing by a gradient pulse depends on the difference in resonance frequencies for the spins comprising the ZQ coherence. For example, dephasing of a heteronuclear ZQ coherence depends on $(\gamma_I - \gamma_S)B_0$, which is on the order of megahertz, and normally is efficient. In contrast, dephasing of homonuclear ZQ coherence depends on $\Omega_I - \Omega_S$, which is on the order of kilohertz (or even zero for identical spins), and is highly inefficient. Special approaches for dephasing ZQ coherences by combinations of adiabatic pulses and gradient pulses have been described (*43*).

4.3.3.3 Limitations of Pulsed Field Gradients The main limitation of pulsed field gradients for coherence selection is evident from [4.41]: if a coherence pathway $p_i \rightarrow p_f$ is selected by gradient techniques, then the corresponding pathway $-p_i \rightarrow p_f$ cannot be selected simultaneously. As discussed in Section 4.3.4, frequency discrimination in indirect evolution periods requires that the signals be recorded for both the $p_i \rightarrow p_f$ and $-p_i \rightarrow p_f$ pathways (in which p_i is the coherence order during t_1 and $p_f = -1$ for observable magnetization during t_2). In most pulsed

field gradient experiments, signals from the two pathways must be acquired sequentially (i.e., in two separate experiments), with the result that the sensitivity of the pulsed field gradient experiment is reduced by a factor of $2^{1/2}$ compared to the corresponding phase-cycled experiment (*39, 44, 45*).

A second limitation is that the use of pulsed field gradients usually requires lengthening of the pulse sequence. Even with actively shielded gradients, delays on the order of 0.1–1.0 ms may be required to permit the spectrometer system to stabilize following a gradient pulse. Additional spin echo sequences also may be necessary to refocus the effects of chemical shift evolution arising from the unperturbed Larmor frequency during a gradient pulse [3.128]. Inevitable relaxation during the inserted delays reduces sensitivity.

4.3.4 FREQUENCY DISCRIMINATION

As noted in Section 4.3.3, coherence order is a signed quantity. The sign indicates the sense of precession of the coherence relative to a reference frame rotating at the transmitter frequency. Differentiating between evolution frequencies higher or lower than the transmitter frequency is called *frequency discrimination* or *quadrature detection* (Section 3.2.2). In high-resolution multidimensional NMR spectroscopy, spectra are desired in which frequency discrimination is obtained and optimal lineshapes are retained in all dimensions. Methods that have been designed to achieve frequency discrimination during indirect evolution periods are outlined in the following discussion. The two basic techniques for frequency discrimination during evolution periods are termed the *hypercomplex* (or *States*) method and the *time-proportional phase-incrementation* (TPPI) method. The analysis here is based on the work of Bodenhausen (*26, 46*) and on the seminal paper by Keeler and Neuhaus (*47*). The following discussion considers two-dimensional spectroscopy; extension to higher dimensions is straightforward.

As discussed in Section 3.2.2, frequency discrimination during the acquisition period is obtained by quadrature detection: the sine- and cosine-modulated components of the evolving magnetization are recorded independently by orthogonal detectors (the exact method depends upon the construction of the spectrometer) and treated as a complex signal during subsequent processing. Conventional quadrature detection cannot be used to determine the relative sense of precession of magnetization in the t_1 dimension of a two-dimensional experiment, because the signal during t_1 is never actually recorded. Nonetheless, the fundamental result that both cosine- and sine-modulated components of

the appropriate coherences must be recorded is equally valid for the indirect evolution period as for the acquisition period.

To continue with the analysis, some important and useful relationships must be developed. Adopting the conventions and notations of Keeler and Neuhaus, the *cosine-modulated* time-domain (t_1) function $S_c(t_1, t_2)$ is

$$\begin{aligned} S_c(t_1, t_2) &= \cos(\Omega_1 t_1)\, \exp(i\Omega_2 t_2) \\ &= \left(\frac{1}{2}\right)[\exp(i\Omega_1 t_1) + \exp(-i\Omega_1 t_1)]\, \exp(i\Omega_2 t_2). \end{aligned} \quad [4.44]$$

Here Ω_1 and Ω_2 are the chemical shifts in the first and second dimensions, respectively. The *sine-modulated* time domain (t_1) function, $S_s(t_1, t_2)$, is

$$\begin{aligned} S_s(t_1, t_2) &= \sin(\Omega_1 t_1)\, \exp(i\Omega_2 t_2) \\ &= -\left(\frac{i}{2}\right)[\exp(i\Omega_1 t_1) - \exp(-i\Omega_1 t_1)]\, \exp(i\Omega_2 t_1). \end{aligned} \quad [4.45]$$

In both $S_c(t_1, t_2)$ and $S_s(t_1, t_2)$, the evolution during the t_1 period modulates the *amplitude* of the signal recorded during t_2. Data in which evolution during the t_1 period modulates the phase of the signal recorded during t_2 are referred to as *P*-type and *N*-type signals, respectively:

$$S_P(t_1, t_2) = \exp[i(\Omega_2 t_2 + \Omega_1 t_1)], \quad [4.46]$$

$$S_N(t_1, t_2) = \exp[i(\Omega_2 t_2 - \Omega_1 t_1)]. \quad [4.47]$$

In *P*-type modulation, the sense of the frequency modulation is the same in t_1 and t_2, whereas in *N*-type modulation, the sense of the frequency modulation is opposite in t_1 and t_2 (*48, 49*). The following relationships are obtained trivially:

$$S_c(t_1, t_2) = [S_P(t_1, t_2) + S_N(t_1, t_2)]/2, \quad [4.48]$$

$$S_s(t_1, t_2) = -i[S_P(t_1, t_2) - S_N(t_1, t_2)]/2. \quad [4.49]$$

For amplitude-modulated signals, the precession of magnetization during t_1 is described by a superposition of two complex signals with opposite frequency, Ω_1 and $-\Omega_1$. These signals result from evolution of the shift operators I^- and I^+, respectively, which in turn correspond to the coherence levels $p = -1$ and $p = +1$ (more generally, for multiple-quantum coherences of order p_i during t_1, $p = p_i$ and $p = -p_i$). Amplitude-modulated data sets require that both positive and negative coherence levels are selected during t_1. In contrast, for phase-modulated signals, precession of magnetization during t_1 is described by a complex signal,

with frequency given by either Ω_1 (for *P*-type signals) or $-\Omega_1$ (for *N*-type signals). These signals result from selection of only one of the coherence levels $p=-1$ or $p=+1$ during t_1 (more generally, for multiple quantum coherences of order p_i during t_1, $p=p_i$ or $p=-p_i$).

The Fourier transform of the function $\exp(i\Omega t - R_2 t)$ is given by (Section 3.3.1)

$$\mathcal{F}\{\exp(i\Omega t - R_2 t)\} = A + iD, \qquad [4.50]$$

in which

$$A = \frac{R_2}{(\omega - \Omega)^2 + R_2^2} \qquad [4.51]$$

is an absorptive Lorentzian line and

$$D = \frac{\omega - \Omega}{(\omega - \Omega)^2 + R_2^2} \qquad [4.52]$$

is a dispersive Lorentzian line, and relaxation of the form $\exp(-R_2 t)$ has been assumed. The shorthand notation A_2, D_2 and A_1, D_1 will be used to represent the absorption and dispersion parts of the signal in the F_2 and F_1 dimensions, respectively. Depending on whether the peaks are located at $+\Omega_1$ or $-\Omega_1$ in the F_1 dimension, the signals will be noted as A_1^+, D_1^+ or A_1^-, D_1^-, respectively.

Fourier transformation of [4.44] with respect to t_2 yields

$$S_c(t_1, F_2) = [\exp(i\Omega_1 t_1) + \exp(-i\Omega_1 t_1)][A_2 + iD_2]/2. \qquad [4.53]$$

Performing a real (cosine) Fourier transform of [4.53] with respect to t_1 yields the two-dimensional spectrum:

$$S_c(F_1, F_2) = [A_1^+ A_2 + A_1^- A_2]/2. \qquad [4.54]$$

Alternatively, if the imaginary part of [4.53] is discarded to give S'_c,

$$S'_c(t_1, F_2) = [\exp(i\Omega_1, t_1) + \exp(-i\Omega_1 t_1)]A_2/2, \qquad [4.55]$$

and a complex Fourier transform of [4.55] is performed with respect to t_1, then the real part of the resulting spectrum is exactly as represented by [4.54]. Equation [4.54] represents two signals, one at $+\Omega_1$, the other at $-\Omega_1$, that are absorptive in both dimensions, as shown in Fig. 4.14a.

Fourier transformation of [4.45] with respect to t_2 yields

$$S_s(t_1, F_2) = -i[\exp(i\Omega_1 t_1) - \exp(-i\Omega_1 t_1)][A_2 + iD_2]/2. \qquad [4.56]$$

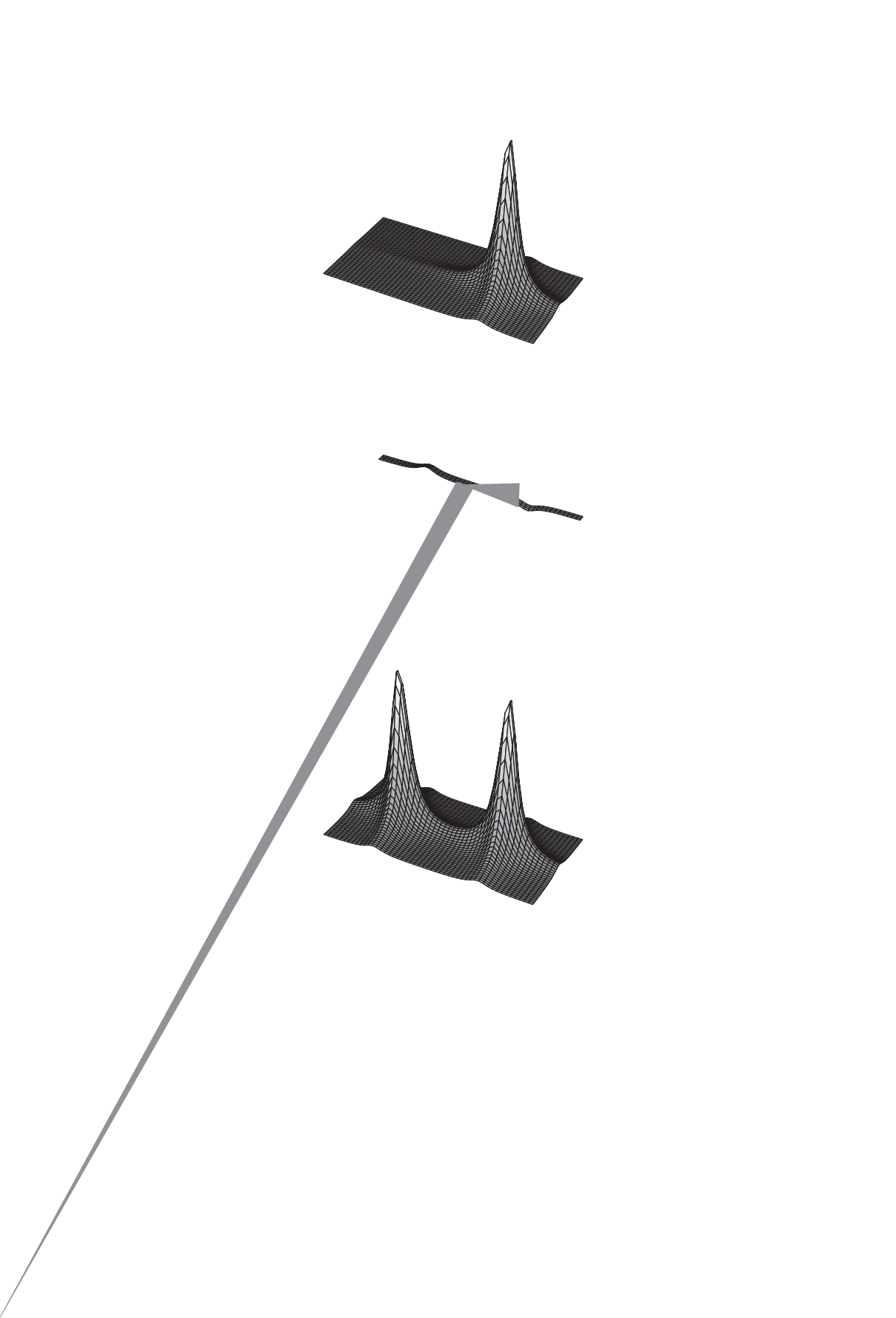

Performing a real Fourier transform of [4.56] with respect to t_1 yields the two-dimensional spectrum:

$$S_s(F_1, F_2) = -i[A_1^+ A_2 - A_1^- A_2]/2. \qquad [4.57]$$

Alternatively, if the imaginary part of [4.56] is discarded to give S_s',

$$S_s'(t_1, F_2) = -i[\exp(i\Omega_1 t_1) - \exp(-i\Omega_1 t_1)]A_2/2, \qquad [4.58]$$

and a complex Fourier transform of [4.58] is performed with respect to t_1, then the real part of the resulting spectrum is exactly as represented by [4.57]. Equation [4.57] represents two signals, one at $+\Omega_1$, the other at $-\Omega_1$, that are absorptive in both dimensions; however, one peak is *positive* and the other is *negative* (Fig. 4.14b).

Combining the results of [4.54] and [4.57] as a complex pair generates a frequency-discriminated spectrum of the form

$$S(F_1, F_2) = S_c(F_1, F_2) + iS_s(F_1, F_2) = A_1^+ A_2, \qquad [4.59]$$

which provides frequency discrimination with retention of a pure double-absorption lineshape. The process is shown schematically in Fig. 4.14.

In contrast, two-dimensional Fourier transformations of [4.46] and [4.47] with respect to t_1 and t_2 yield

$$\begin{aligned} S_P(F_1, F_2) &= [A_1^- + iD_1^-][A_2 + iD_2] \\ &= [A_1^- A_2 - D_1^- D_2] + i[A_1^- D_2 + D_1^- A_2], \end{aligned} \qquad [4.60]$$

$$\begin{aligned} S_N(F_1, F_2) &= [A_1^+ - iD_1^+][A_2 + iD_2] \\ &= [A_1^+ A_2 + D_1^+ D_2] + i[A_1^+ D_2 - D_1^+ A_2]. \end{aligned} \qquad [4.61]$$

The real parts of these spectra represent frequency-discriminated spectra, as desired; however, the lineshape is a superposition of doubly absorptive and doubly dispersive signals. This lineshape is called *phase twisted* and is extremely undesirable in high-resolution NMR spectroscopy because the dispersive tails in the lineshape degrade the resolution in the spectrum. The *P* and *N* signals are phase twisted in the opposite sense. Absorption and phase-twisted lineshapes are compared in Fig. 4.15. As will be seen in Section 4.3.4.2, [4.48] and [4.49] can be used to generate amplitude-modulated data from separately recorded *P*-type and *N*-type signals, and the resulting amplitude-modulated data can be used to generate a phase-sensitive spectrum, as previously described.

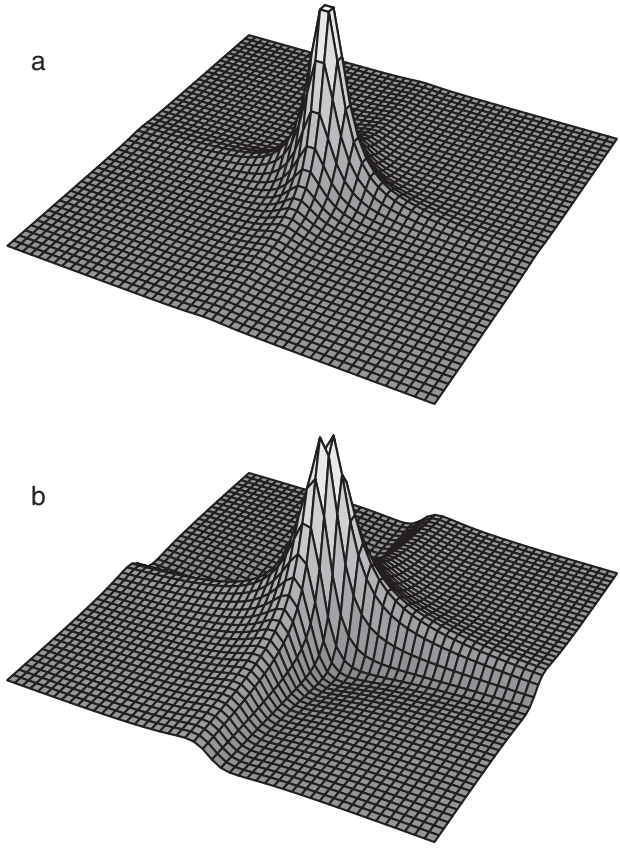

FIGURE 4.15 Comparison of (a) absorptive and (b) phase-twisted lineshapes.

4.3.4.1 Frequency Discrimination by Phase Cycling Both positive and negative coherence levels are selected during t_1 in a natural fashion in phase-cycled experiments by using the periodicity of phase-cycled coherence filters to select both desired pathways simultaneously. The practical problem is then to separately record the two data sets $S_c(t_1, t_2)$ and $S_s(t_1, t_2)$. The key is to recognize that, if a given pulse sequence selects a coherence of order p during t_1 and results in a cosine-modulated signal, then the sine-modulated signal is recorded in a second experiment by shifting the phase of an appropriate pulse sequence element (usually preceding the evolution period) by $\pi/(2|p|)$ [4.35].

In the hypercomplex (*50*) method, cosine- and sine-modulated data sets are recorded using a sampling interval in t_1 of $1/SW_1$, where SW_1

is the required spectral width in the F_1 dimension, and are processed exactly as previously described. The combination of the two separate data sets can be performed before the second complex Fourier transform (with respect to t_1), because the Fourier transform is linear.

An alternative method was designed by Marion and Wüthrich (*51*). This procedure achieves identical results but employs real Fourier transformations. The idea finds its roots in Redfield's method for quadrature-detected spectra using a single analog-to-digital converter (ADC) (*52*). Some NMR instruments were originally designed with only one ADC, rather than two, as this was deemed an expensive component. One-dimensional quadrature detection on such spectrometers requires recording data points every 1/(2SW), where SW is the spectral width, twice the normal rate of data acquisition. In addition, the phase of the receiver is incremented by 90° after each data point is recorded. For this reason, the method is known as *time-proportional phase incrementation* (TPPI). The spectrum is subsequently obtained by application of a real Fourier transform. Overall, the effect of the TPPI procedure is to add a frequency of SW/2 to each data point in the transformed spectrum, thus achieving frequency discrimination. Those peaks in the spectrum below the transmitter frequency (at zero), between −SW/2 and zero, are shifted to between zero and SW/2, while those peaks between zero and +SW/2 are shifted to between +SW/2 and SW. Therefore, all resonances in the spectrum appear with the same sign of precession.

The same method can be employed in two-dimensional NMR spectroscopy. The incrementable period, t_1, is incremented in steps of $1/(2SW_1)$. Between each successive t_1 increment, the phase of the coherence during t_1 is shifted by 90° (by shifting the phases of the pulses prior to t_1 appropriately). Consider the effect of this phase incrementation for the odd and even t_1 increments for a sampling interval of $\Delta t_1 = 1/(2SW_1)$. For example, assume the odd-numbered data points sample the cosine-modulated signal $\cos(\Omega_1 t_1)$ and the even-numbered data points sample the sine-modulated signal $\sin(\Omega_1 t_1)$, where Ω_1 is the frequency of the coherence of interest evolving during the t_1 period. Consequently, the sampled data set is described by the series over the integer index $m \geq 1$:

$$S[(m-1)\Delta t_1] = 1,\ \sin(\Omega_1 \Delta t_1),\ -\cos(\Omega_1 2\Delta t_1),\ -\sin(\Omega_1 3\Delta t_1),\ \cos(\Omega_1 4\Delta t_1), \ldots . \qquad [4.62]$$

The alternating signs of the cosine and sine terms result from the phase incrementation procedure. This series of data samples is represented in a

compact form as

$$\begin{aligned} S[(m-1)\Delta t_1] &= \cos[(\Omega_1 - 2\pi/4\Delta t_1)(m-1)\Delta t_1] \\ &= \cos[(\Omega_1 - \Omega_{\mathrm{TPPI}})(m-1)\Delta t_1], \end{aligned} \quad [4.63]$$

in which $\Omega_{\mathrm{TPPI}}/2\pi = \mathrm{SW}_1/2$. Real Fourier transformation of this data set produces a spectrum with a signal at the apparent frequency $\Omega_1 - \Omega_{\mathrm{TPPI}}$. Thus, the TPPI procedure eliminates the need for explicit discrimination of the signs of the coherence frequencies within the unaliased bandwidth by shifting the effective reference frequency to one edge of the spectrum, resulting in all of the frequencies having the same sign. This procedure is analogous to that proposed by States and co-workers; in particular, the TPPI method requires exactly the same total number of transients and total acquisition time as does the States (or hypercomplex) method. In order to avoid baseline distortion, use of the TPPI procedure requires that the coherences be represented in the form $\cos(\Omega_1 t_1 + \phi)$, where ϕ is an integral multiple of $\pi/2$ (in other words, the resulting spectrum needs either 0° or 90° zero-order phase correction (Section 4.3.4.3) (*53*). In principle, a TPPI procedure can be superimposed on the hypercomplex quadrature scheme to achieve an apparent frequency shift in an indirect dimension of a multidimensional experiment. In most cases, physically shifting the rf transmitter frequency (assuming the shift can be done phase coherently if necessary) is preferable in order to minimize resonance offset effects.

Salient features of the States (hypercomplex), TPPI, and hybrid TPPI–States (*54*) protocols are summarized in Table 4.5. Although the discussions and derivations here have been applied solely to two-dimensional NMR spectroscopy, the methods are equally applicable to higher dimensional experiments.

4.3.4.2 Frequency Discrimination by Pulsed Field Gradients

Coherence selection by pulsed field gradients naturally results in *P*-type or *N*-type modulation of the observed signal. Either *P*-type or *N*-type data are selected, depending on the relative sense of the initial dephasing gradient pulse and the final, refocusing gradient. To obtain frequency-discriminated phase-sensitive spectra by using the gradient approach, both the *P*-type and the *N*-type data are recorded separately (*39, 44, 45*). Cosine- and sine-modulated data are obtained by combining the *P*- and *N*-type data using [4.48] and [4.49]. The resulting amplitude-modulated data are processed as complex data by using the States method of frequency discrimination.

TABLE 4.5
Quadrature Detection Methods[a]

Experiment	Increment	Pulse phase	Receiver phase
	TPPI		
$(4k+1)$	$t_1(0)+(4k)\Delta$	x	x
$(4k+2)$	$t_1(0)+(4k+1)\Delta$	y	x
$(4k+3)$	$t_1(0)+(4k+2)\Delta$	$-x$	x
$(4k+4)$	$t_1(0)+(4k+3)\Delta$	$-y$	x
	States		
$(4k+1)$	$t_1(0)+(4k)2\Delta$	x	x
$(4k+2)$	$t_1(0)+(4k)2\Delta$	y	x
$(4k+3)$	$t_1(0)+(4k+1)2\Delta$	x	x
$(4k+4)$	$t_1(0)+(4k+1)2\Delta$	y	x
	TPPI–States		
$(4k+1)$	$t_1(0)+(4k)2\Delta$	x	x
$(4k+2)$	$t_1(0)+(4k)2\Delta$	y	x
$(4k+3)$	$t_1(0)+(4k+1)2\Delta$	$-x$	$-x$
$(4k+4)$	$t_1(0)+(4k+1)2\Delta$	$-y$	$-x$

[a] The index $k=0,1,\ldots,N/4-1$, in which N is the number of experiments acquired in the t_1 dimension, and $\Delta=1/(2SW_1)$. The initial sampling delay is $t_1(0)$ and is usually set to 0 or Δ. The t_1 interferogram consists of N real points for the TPPI method and $N/2$ complex points for the States and TPPI–States methods. The t_1 increment is twice as large for the States and TPPI–States methods as for the TPPI method, but SW_1 and t_{1max} are identical for all methods.

Although this procedure produces frequency discrimination in the indirect dimension of the spectrum while keeping absorption lineshapes, the signal-to-noise ratio is reduced by a factor of $2^{1/2}$ compared to the phase-cycled approaches to frequency discrimination. However, in many experiments, this reduction is avoided by the use of so-called PEP (preservation of equivalent pathways) experiments described in Chapter 7 (Section 7.1.3.3).

4.3.4.3 Aliasing, Folding, and Phasing in Multidimensional NMR Spectroscopy The location of axial peaks in a multidimensional NMR spectrum depends upon the manner in which frequency discrimination is performed in the F_1 dimension. If the hypercomplex (States) method is used, then the axial peaks occur at $F_1=0$ and result in a ridge of axial peaks across the center of the spectrum, parallel to the F_2 axis. If the TPPI method is used, then the axial peaks occur at the edge of the spectrum for the following reason. The TPPI phase cycle adds a

frequency Ω_{TPPI} to the resonance frequencies in F_1; however, the axial peaks are unaffected by the phase cycle and consequently appear in the spectrum at the apparent frequency $-\Omega_{TPPI}$. Generally, even if axial peak suppression phase cycling is employed, placement of axial peaks at the edge of the spectrum minimizes artifacts. The hybrid TPPI–States protocol is identical to the conventional States method except that the axial peaks are shifted to the edge of the spectrum.

As described in Section 3.2.1, resonance frequencies outside the spectral width appear artifactually within the spectral width. For complex data (States or TPPI–States frequency discrimination), resonance signals are aliased: signals upfield (downfield) of the edge of the spectral region appear in the downfield (upfield) spectral region. The apparent resonance frequency, ν_a, and the true resonance frequency, ν_0, are related by

$$\nu_a = \nu_0 - mSW, \qquad [4.64]$$

in which m is an integer equal to the number of times the signal has been aliased. For real data (TPPI frequency discrimination), resonance signals are folded: signals upfield (downfield) of the edge of the spectral region reflect back across the upfield (downfield) edge of the spectral region. The apparent resonance frequency, ν_a, and the true resonance frequency, ν_0, are related by

$$\nu_a = (-1)^m(\nu_0 - mSW). \qquad [4.65]$$

Aliasing and folding (*55*) are illustrated in Fig. 4.16. Aliasing is useful particularly for minimizing the spectral width in heteronuclear NMR experiments and is discussed further in Section 7.1.2.5.

Distortions in the baseline caused by phase correction (Section 3.3.2.3) are particularly serious problems in multidimensional NMR spectroscopy. Fortunately, the receiver reference phase can be easily adjusted on modern NMR spectrometers in order to set the initial signal phase (usually equal to zero). A number of experimental techniques have been developed to ensure that the initial sampling delay in the acquisition dimension $t_0 = 0$ or $t_0 = 1/(2SW)$. For example, the Hahn echo sequence can be used to adjust the initial sampling delay (Section 3.6.4.2). Adjustment of the initial sampling delay for indirectly detected evolution periods in multidimensional NMR experiments must account for phase evolution during the preparation and mixing periods. The accrued phase depends upon chemical shift evolution during the evolution period and phase evolution during off-resonance rf pulses within or flanking the evolution period.

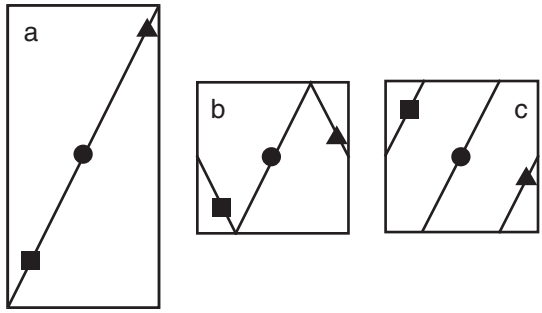

FIGURE 4.16 Folding and aliasing in the F_1 dimension. (a) Schematic spectrum with a full spectral width. (b) The F_1 spectral width is halved and frequency discrimination is performed using real (TPPI) acquisition. Resonances outside the spectral width are folded into the spectrum. (c) The F_1 spectral width is halved and frequency discrimination is performed using hypercomplex (States or TPPI–States) acquisition. Resonances outside the spectral width are aliased into the spectrum.

Complex (States, States–TPPI, echo/antiecho) frequency discrimination is considered first. The pulse sequence element $90°$–t_1–$90°$ is encountered frequently in homonuclear multidimensional pulse sequences. Utilizing the expression for phase evolution during rf pulses given by [3.70], to ensure an initial sampling delay of $t_0 = 1/(2\mathrm{SW}_1)$, the initial value of t_1 must be set to

$$t_1(0) = 1/(2\mathrm{SW}_1) - 4\tau_{90}/\pi, \qquad [4.66]$$

in which τ_{90} is the length of a $90°$ pulse. If an initial sampling delay of zero is desired, then the pulse sequence element $90°$–t_1– –$180°$– –$90°$, in which is a fixed delay, can be used. The $180°$ pulse refocuses the effects of phase evolution during the flanking $90°$ pulses; thus

$$t_1(0) = \left\{ \begin{array}{c} 0 \\ 1/(2\mathrm{SW}_1) \end{array} \right\} \qquad [4.67]$$

can be chosen as desired. In heteronuclear correlation NMR experiments, the pulse sequence element $90°(S)$–$t_1/2$–$180°(I)$–$t_1/2$–$90°(S)$ commonly is used to decouple I and S spins during the evolution period. In this case, the initial value of t_1 must be set to

$$t_1(0) = 1/(2\mathrm{SW}_1) - 4\tau_{90(\mathrm{S})}/\pi - \tau_{180(\mathrm{I})} \qquad [4.68]$$

to ensure $t_0 = 1/(2SW_1)$. Processing details for $t_0 = 0$ or $t_0 = 1/(2SW_1)$ are discussed in Section 3.3.2.3.

For real (TPPI) frequency discrimination, an additional consideration arises. The real signal can be written as the sum of two complex exponential signals. Thus, assuming an initial sampling delay $t_0 = 0$,

$$\begin{aligned} s(j\Delta t) &= I_0 \cos[\Omega j\Delta t + \phi_0] \exp[-\lambda_0 j\Delta t] \\ &= (1/2)I_0\{\exp[(i\Omega - \lambda_0)j\Delta t + i\phi_0] + \exp[(-i\Omega - \lambda_0)j\Delta t - i\phi_0]\}. \end{aligned} \quad [4.69]$$

The transformed spectrum, obtained by analogy to [3.53], is

$$S(\omega_k) \approx \frac{-I_0}{2\Delta t}\left\{\frac{1}{(i\Omega - i\omega_k - \lambda_0)} + \frac{1}{(-i\Omega - i\omega_k - \lambda_0)}\right\} + \frac{I_0}{2}\cos\phi_0. \quad [4.70]$$

The baseline offset term vanishes if $\phi_0 = \pm\pi/2$. In this case, [4.69] becomes

$$s(j\Delta t) = \pm I_0 \sin[\Omega j\Delta t] \exp[-\lambda_0 j\Delta t] \quad [4.71]$$

and the signal is said to be sine modulated. If the indirect evolution period has the form 90°_ϕ–t_1–90°_x, then sine-modulated data with $t_0 = 0$ is obtained by the following procedure. The first FID is acquired with an initial sampling point set according to [4.66] and $\phi = x$. The interferogram is sampled using the TPPI method applied to the phase ϕ. After acquisition and processing in the acquisition dimension, a zero value is preappended to the beginning of the interferogram (typically by right shifting the data vector) prior to processing the indirect dimension. A 90° zero-order phase correction is applied after Fourier transformation.

4.4 Resolution and Sensitivity

The sensitivity of a multidimensional spectrum is close to that of an equivalent one-dimensional experiment recorded in the same total experiment time. Although a particular peak may appear only weakly in each F_2 spectrum (recorded for each t_1 value), the Fourier transform with respect to t_1 concentrates all the signal into a few points in the final multidimensional spectrum. In effect, the signal-to-noise ratio of a peak in the multidimensional spectrum is a function of the time-average signal throughout the *entire* multidimensional NMR experiment.

Three factors lead to a reduction in sensitivity of multidimensional spectra when compared to their one-dimensional counterparts: (*i*)

relaxation during the incrementable time periods results in a progressive loss of signal as the variable delay increases, (*ii*) cancellation of antiphase signals due to overlap (Section 6.2.1.5), and (*iii*) the integrated intensity of a single peak in the one-dimensional spectrum is associated with several peaks in the multidimensional spectrum (i.e., diagonal and cross-peaks). The trade-off between sensitivity and resolution is the same as for one-dimensional spectroscopy: more t_1 increments must be recorded to increase resolution ($t_{1\max}$); however, relaxation during the added t_1 time periods causes the signal decay and loss of sensitivity.

Because the signal nearly always is truncated in the incrementable time periods of multidimensional NMR experiments, suitable apodization functions must be applied to generate spectra containing the required information. Such functions and their effects on truncated data are discussed in Section 3.3.2.2.

4.5 Three- and Four-Dimensional NMR Spectroscopy

Two-dimensional NMR spectroscopy has proved to be one of the most important developments in high-resolution NMR. However, for proteins with masses greater than 10 to 12 kDa, even the increased resolution of the two-dimensional spectra is insufficient, and so alternative approaches have been sought.

The approach that has now become widely adopted is to increase the number of frequency dimensions possessed by the spectrum. The principles and fundamental ideas already discussed for two-dimensional NMR extend into higher dimensional experiments: the same types of magnetization transfer processes are active, the same principles concerning coherence selection, quadrature detection, resolution, and sensitivity are applicable, and product operator analyses are employed in the same way. Higher dimensional experiments are built from combinations of two-dimensional experiments and can combine the magnetization transfer capabilities of both dipolar and scalar coupling interactions in the same sequence.

Three-dimensional pulse sequences are derived from a combination of two two-dimensional pulse sequences (*56–58*), as shown schematically in Fig. 4.17. The acquisition period of the first pulse sequence and the preparation period of the second pulse sequence are omitted in concatenating the two experiments. In three-dimensional experiments, the signal is recorded conventionally during an acquisition time, denoted t_3, as a function of *two* evolution times, t_1 and t_2, which are incremented independently from one experiment to another. This procedure generates

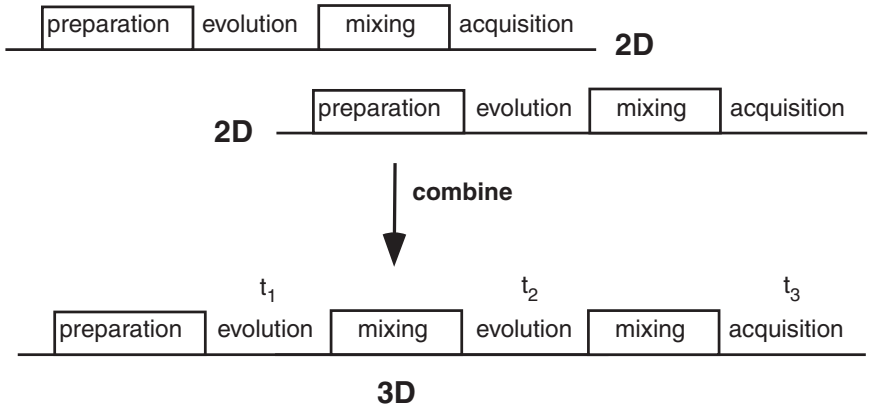

FIGURE 4.17 Schematic generation of a three-dimensional NMR experiment from the combination of two two-dimensional NMR experiments. The mixing period of one two-dimensional experiment and the preparation period of a second two-dimensional experiment are combined. The three-dimensional experiment contains three independent time periods. The FID is recorded during the acquisition time, t_3, as a function of two independently incremented evolution times, t_1 and t_2. A mixing period follows each evolution time, causing a potential two-step magnetization transfer process.

a three-dimensional time-domain data matrix to which a three-dimensional Fourier transformation is applied. The corresponding frequency dimensions are denoted F_1, F_2, and F_3. The spectrum can be represented as a three-dimensional cube, but analysis of a three-dimensional spectrum is more convenient if two-dimensional slices are taken from the cube as shown in Fig. 4.18. In this case the *tiers* or *planes* from the cube are seen as sets of two-dimensional spectra (F_3, F_1) separated by another interaction along the F_2 dimension.

Again, as in two-dimensional spectroscopy, either similar or different nuclear types can appear in different dimensions, as required, and correlations between the separate dimensions can be established via NOE effects or through scalar couplings. Those experiments in which all three dimensions contain ^{1}H chemical shifts or couplings are referred to as homonuclear three-dimensional experiments. Those experiments in which one or more dimension is not ^{1}H (usually ^{13}C and/or ^{15}N) are referred to as heteronuclear three-dimensional experiments. Analyses of the most important three-dimensional methods for biological studies are presented in Chapters 6, 7 and 9.

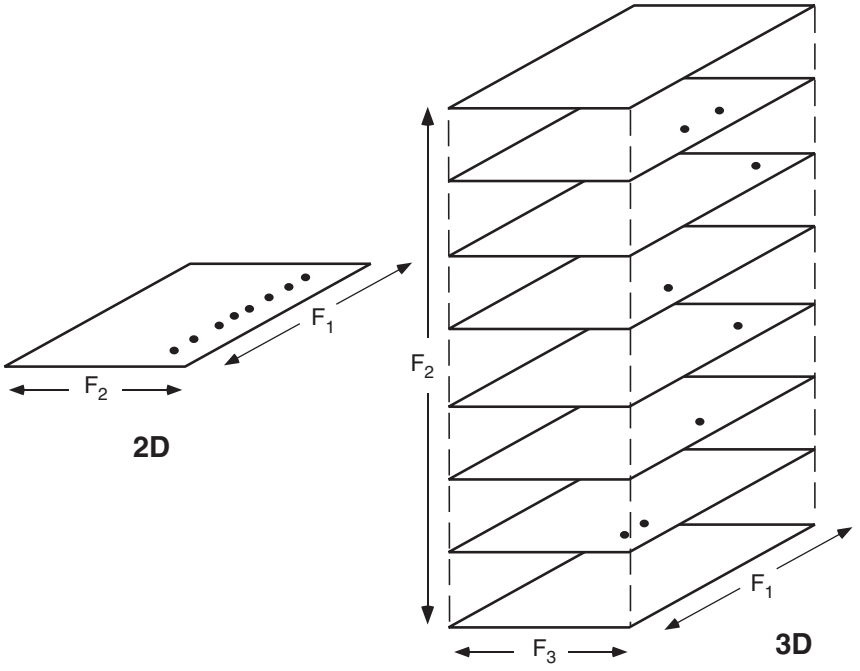

FIGURE 4.18 The development of a three-dimensional data set from a two-dimensional data set. The two-dimensional data set depicted here shows a set of resonances that, although resolved in the F_1 dimension, are not clearly determined in the F_2 dimension. The introduction of an additional evolution period generates a third frequency dimension perpendicular to the first two. The increased resolution afforded by virtue of a second magnetization transfer step can alleviate ambiguities in the two-dimensional spectrum.

In a similar fashion, a four-dimensional experiment consists of a combination of three two-dimensional sequences, omitting the detection periods of the first and second experiments and the preparation stages of the second and third experiments (*59*). As shown in Fig. 4.19, the general experiment contains three independently incrementable time periods (t_1, t_2, t_3) and the acquisition time period, t_4, and consequently the resulting data are a function of these four time periods. Four-dimensional experiments are used in those cases when there is still ambiguity arising due to degeneracy and overlap even in three-dimensional spectra. Up to this point in time, four-dimensional experiments have been exclusively

FIGURE 4.19 A schematic representation of a four-dimensional NMR experiment. The four-dimensional experiment contains four independent time periods. The FID is recorded during the acquisition time, t_4, as a function of three independently incremented evolution times, t_1, t_2, and t_3. A mixing period follows each evolution period, causing a potential three-step magnetization transfer process.

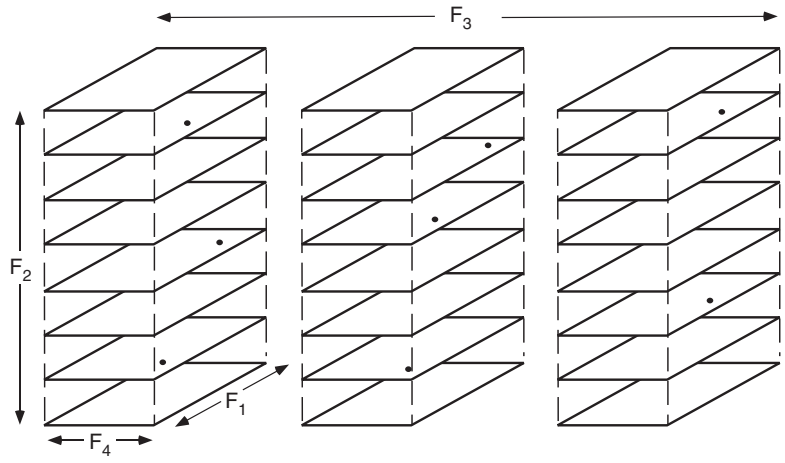

FIGURE 4.20 A four-dimensional experiment is visualized as a series of three-dimensional cubes. Each cube represents the three-dimensional F_1, F_2, F_4 subspectrum for a different value of F_3.

heteronuclear techniques. Detailed discussions of some useful four-dimensional experiments are presented in Chapters 7 and 9.

Visualizing a four-dimensional spectrum can be difficult, although one convenient method is to imagine each two-dimensional slice of a three-dimensional spectrum expanded into an additional dimension by another type of interaction. The progression from two-dimensional spectra to four-dimensional spectra is represented schematically by Fig. 4.20.

References

1. R. Freeman, W. A. Anderson, *J. Chem. Phys.* **37**, 2053–2073 (1962).
2. R. A. Hoffman, S. Forsén, *Prog. NMR Spectrosc.* **1**, 15–204 (1966).
3. D. Neuhaus, M. Williamson, "The Nuclear Overhauser Effect in Structural and Conformational Analysis," pp. 1–522. VCH Publishers, New York, 1989.
4. J. H. Noggle, R. E. Shirmer, "The Nuclear Overhauser Effect: Chemical Applications," pp. 1–259 Academic Press, New York, 1971.
5. R. R. Ernst, *J. Chem. Phys.* **45**, 3845–3861 (1966).
6. W. A. Anderson, R. Freeman, *J. Chem. Phys.* **37**, 85–103 (1962).
7. W. A. Anderson, F. A. Nelson, *J. Chem. Phys.* **39**, 183–189 (1963).
8. J. Jeener, Ampère Summer School, Basko Polje, Yugoslavia, 1971.
9. W. P. Aue, E. Bartholdi, R. R. Ernst, *J. Chem. Phys.* **64**, 2229–2246 (1976).
10. J. Jeener, in "NMR and More, in Honour of Anatole Abragam" (M. Goldman, M. Porneuf, eds.), pp. 1–388. Les Editions de Physique, Les Ulis, France, 1994.
11. L. Braunschweiler, R. R. Ernst, *J. Magn. Reson.* **53**, 521–528 (1983).
12. S. R. Hartmann, E. L. Hahn, *Phys. Rev.* **128**, 2042–2053 (1962).
13. L. Müller, R. R. Ernst, *Mol. Phys.* **38**, 963–992 (1979).
14. R. Bazzo, I. D. Campbell, *J. Magn. Reson.* **76**, 358–361 (1988).
15. M. Rance, *J. Magn. Reson.* **74**, 557–564 (1987).
16. A. Bax, D. G. Davis, *J. Magn. Reson.* **65**, 355–360 (1985).
17. J. Jeener, B. H. Meier, P. Bachmann, R. R. Ernst, *J. Chem. Phys.* **71**, 4546–4553 (1979).
18. G. A. Morris, R. Freeman, *J. Am. Chem. Soc.* **101**, 760–762 (1979).
19. D. P. Burum, R. R. Ernst, *J. Magn. Reson.* **39**, 163–168 (1980).
20. D. M. Doddrell, D. T. Pegg, M. R. Bendall, *J. Magn. Reson.* **48**, 323–327 (1982).
21. M. R. Bendall, D. T. Pegg, *J. Magn. Reson.* **53**, 272–296 (1983).
22. K. E. Kover, G. Batta, *Prog. NMR Spectrosc.* **19**, 223–266 (1987).
23. M. W. F. Fischer, L. Zeng, E. R. P. Zuiderweg, *J. Am. Chem. Soc.* **118**, 12457–12458 (1996).
24. M. R. Hansen, M. Rance, A. Pardi, *J. Am. Chem. Soc.* **120**, 11210–11211 (1998).
25. J. Keeler, in "Multinuclear Magnetic Resonance in Liquids and Solids — Chemical Applications" (P. Granger, R. K. Harris, eds.), pp. 103–129, Vol. 322. NATO ASI Series C. Kluwer Academic Press, Netherlands, 1990.
26. G. Bodenhausen, H. Kogler, R. R. Ernst, *J. Magn. Reson.* **58**, 370–388 (1984).
27. M. H. Levitt, P. K. Maduh, C. E. Hughes, *J. Magn. Reson.* **155**, 300–306 (2002).
28. C. E. Hughes, M. Carravetta, M. H. Levitt, *J. Magn. Reson.* **167**, 259–265 (2004).
29. D. I. Hoult, *Proc. Roy. Soc. Lond., Ser. A* **344**, 311–340 (1975).
30. G. Bodenhausen, R. Freeman, D. L. Turner, *J. Magn. Reson.* **26**, 373–378 (1977).
31. R. E. Hurd, *J. Magn. Reson.* **87**, 422–428 (1990).
32. R. E. Hurd, B. K. John, *J. Magn. Reson.* **92**, 658–668 (1991).
33. R. E. Hurd, B. K. John, *J. Magn. Reson.* **91**, 648–653 (1991).
34. A. Bax, P. G. D. Jong, A. F. Mehlkopf, J. Smidt, *Chem. Phys. Lett.* **69**, 567–570 (1980).
35. P. Barker, R. Freeman, *J. Magn. Reson.* **64**, 334–338 (1985).
36. G. W. Vuister, R. Boelens, R. Kaptein, R. E. Hurd, B. John, P. C. M. van Zijl, *J. Am. Chem. Soc.* **113**, 9688–9690 (1991).
37. G. W. Vuister, R. Boelens, R. Kaptein, M. Burgering, P. C. M. van Zijl, *J. Biomol. NMR.* **2**, 301–305 (1992).
38. B. K. John, D. Plant, P. Webb, R. E. Hurd, *J. Magn. Reson* **98**, 200–206 (1992).
39. A. L. Davis, J. Keeler, E. D. Laue, D. Moskau, *J. Magn. Reson.* **98**, 207–216 (1992).

40. A. L. Davis, E. D. Laue, J. Keeler, D. Moskau, J. Lohman, *J. Magn. Reson.* **94**, 637–644 (1991).
41. J. Keeler, R. T. Clowes, A. L. Davis, E. D. Laue, *Meth. Enzymol.* **239**, 145–207 (1994).
42. A. Bax, S. S. Pochapsky, *J. Magn. Reson.* **99**, 638–643 (1992).
43. M. J. Thrippleton, J. Keeler, *Angew. Chem. Int. Ed. Engl.* **42**, 3938–3941 (2003).
44. J. R. Tolman, J. Chung, J. P. Prestegard, *J. Magn. Reson.* **98**, 462–467 (1992).
45. J. Boyd, N. Soffe, B. K. John, D. Plant, R. E. Hurd, *J. Magn. Reson.* **98**, 660–664 (1992).
46. G. Bodenhausen, R. Freeman, R. Niedermeyer, D. L. Turner, *J. Magn. Reson.* **26**, 133–164 (1977).
47. J. Keeler, D. Neuhaus, *J. Magn. Reson.* **63**, 454–472 (1985).
48. K. Nagayama, A. Kumar, K. Wüthrich, R. R. Ernst, *J. Magn. Reson.* **40**, 321–334 (1980).
49. A. Bax, R. Freeman, *J. Magn. Reson.* **44**, 542–561 (1981).
50. D. J. States, R. A. Haberkorn, D. J. Ruben, *J. Magn. Reson.* **48**, 286–292 (1982).
51. D. Marion, K. Wüthrich, *Biochem. Biophys. Res. Commun.* **113**, 967–974 (1983).
52. A. G. Redfield, S. D. Kunz, *J. Magn. Reson.* **19**, 250–254 (1975).
53. D. Marion, A. Bax, *J. Magn. Reson.* **79**, 352–356 (1988).
54. D. Marion, M. Ikura, R. Tschudin, A. Bax, *J. Magn. Reson.* **85**, 393–399 (1989).
55. R. R. Ernst, G. Bodenhausen, A. Wokaun, "Principles of Nuclear Magnetic Resonance in One and Two Dimensions," pp. 1–610. Clarendon Press, Oxford, 1987.
56. C. Griesinger, O. W. Sørensen, R. R. Ernst, *J. Magn. Reson.* **73**, 574–579 (1987).
57. H. Oschkinat, C. Griesinger, P. J. Kraulis, O. W. Sørenson, R. R. Ernst, A. M. Gronenborn, G. M. Clore, *Nature* **332**, 374–376 (1988).
58. C. Griesinger, O. W. Sørensen, R. R. Ernst, *J. Magn. Reson.* **84**, 14–63 (1989).
59. L. E. Kay, G. M. Clore, A. Bax, A. M. Gronenborn, *Science* **249**, 411–414 (1990).